



## Geometry and P and S velocity structure of the “African Anomaly”

Yi Wang<sup>1,2</sup> and Lianxing Wen<sup>1</sup>

Received 3 May 2006; revised 22 October 2006; accepted 8 December 2006; published 26 May 2007.

[1] We constrain the geometry and P and S velocity structure of a low-velocity anomaly in the lower mantle beneath southern Africa (we term it the “African Anomaly”) on the basis of forward traveltimes and waveform modeling of seismic data sampling a great arc across the anomaly from the East Pacific Rise to the Japan Sea. Our collected data set consists of direct S, direct P, Sdiff, ScS, PcP, SKS, and SKKS phases recorded by three temporary broadband PASSCAL seismic arrays deployed in Africa between 1994 and 2002, the Tanzania seismic array (1994–1995), the Kaapvaal seismic array (1997–1999), and the Ethiopia/Kenya seismic array (2000–2002) for earthquakes occurring in the East Pacific Rise, Drake Passage, South Sandwich islands, Iran, Hindu Kush, Xinjiang, and the Japan Sea. The seismic data provide excellent sampling of the African Anomaly in the lower mantle along the specific great arc. In order to accurately account for the contributions from the African Anomaly, we relocate all the events using a global seismic shear velocity tomographic model and seismic data recorded by the Global Seismographic Network and correct for the contributions from the seismic heterogeneities outside the African Anomaly. The seismic observations suggest that the African Anomaly locally extends 1300 km above the core-mantle boundary beneath southern Africa (around  $-25^{\circ}\text{N}$ ,  $27^{\circ}\text{E}$ ) and exhibits a “bell-like” geometry with both the southwestern and the northeastern flanks dipping toward its center with the lateral dimension of the anomaly increasing with depth. The base is about 4000 km wide extending broadly in both the southwestward and the northeastward directions. The seismic data can best be explained by a shear velocity structure with average velocity decreases of  $-5\%$  in the base and  $-2\%$  to  $-3\%$  in the mid-lower mantle above the base, and a compressional velocity structure with a uniform S to P velocity perturbation ratio of 3:1 for the entire African Anomaly. These geometric and velocity features suggest that the mid-lower mantle portion of the African Anomaly is an integral component of the very low velocity province and the African Anomaly is compositionally distinct and geologically stable.

**Citation:** Wang, Y., and L. Wen (2007), Geometry and P and S velocity structure of the “African Anomaly,” *J. Geophys. Res.*, *112*, B05313, doi:10.1029/2006JB004483.

### 1. Introduction

[2] The “African Anomaly” is one of two prominent large-scale low-velocity anomalies (the other one is beneath the central Pacific) in the Earth’s lower mantle [e.g., *Su et al.*, 1992; *Li and Romanowicz*, 1996; *Masters et al.*, 1996; *Grand et al.*, 1997; *van der Hilst et al.*, 1997; *Ritsema et al.*, 1999]. The African Anomaly has a very low velocity province (VLVP) as its base near the core-mantle boundary (CMB) and regionally extends more than 1000 km upward into the lower mantle. The structural and velocity features of the VLVP are extensively mapped out and the origin of the VLVP is now clear. The VLVP exhibits an “L-shaped”

form changing from a north-south orientation in the South Atlantic Ocean to an east-west orientation in the Indian Ocean, occupying an area of about  $1.8 \times 10^7 \text{ km}^2$  at the CMB. Seismic data also suggest that the VLVP has rapidly varying thicknesses from 300 km to 0 km, steeply dipping edges, and a strong linear gradient of shear velocity reduction from  $-2\%$  (top) to  $-9\%$  to  $-12\%$  (bottom) relative to the Preliminary Reference Earth Model (PREM [*Dziewonski and Anderson*, 1981]) [*Wen et al.*, 2001; *Wen*, 2001; *Wang and Wen*, 2004]. These structural and velocity features unambiguously indicate that the VLVP is compositionally distinct. It has also been suggested that the seismic velocity structure of the VLVP can best be explained by partial melt driven by a compositional change, possibly produced early in the Earth’s history [*Wen et al.*, 2001; *Wen*, 2001; *Wang and Wen*, 2004].

[3] Seismic tomographic studies [*Grand et al.*, 1997; *van der Hilst et al.*, 1997] and the seismic data recorded by the Tanzania seismic array [*Ritsema et al.*, 1998] clearly indi-

<sup>1</sup>Department of Geosciences, State University of New York at Stony Brook, Stony Brook, New York, USA.

<sup>2</sup>Now at CGGVeritas, Houston, Texas, USA.

**Table 1.** Event List

Event	Origin Date Time, UT	Latitude, <sup>a</sup> °N	Longitude, <sup>a</sup> °E	Depth, <sup>a</sup> km	Time Correction, s
EPR97/06/10	97/06/10 2205:19	-35.81 (-35.41)	-108.14 (-108.14)	10	5.4
DP95/01/03	95/01/03 1612:00	-57.70 (-57.40)	-65.96 (-65.96)	33	6.3
SS97/09/05 <sup>b</sup>	97/09/05 0329:05	-56.26 (-56.08)	-27.82 (-27.59)	33	7.5
SS97/10/05 <sup>c</sup>	97/10/05 1809:45	-59.74 (-59.54)	-29.20 (-29.60)	274	2.1
SS95/03/26	95/03/26 0216:16	-55.85 (-55.65)	-28.21 (-28.31)	77	3.9
SS02/02/10	02/02/10 0147:06	-55.91 (-55.91)	-29.00 (-29.10)	193	0.8
SS02/03/09	02/03/09 1227:11	-56.02 (-55.92)	-27.33 (-27.33)	118	2.2
IR98/03/14	98/03/14 1940:27	30.15 (29.85)	57.60 (57.70)	9	6.4
HK97/05/13	97/05/13 1422:48	36.41 (36.31)	70.95 (70.94)	196 (191)	5.7
XJ98/08/27	98/08/27 0903:37	39.66 (39.46)	77.34 (77.34)	33	6.5
JS97/12/05	97/12/05 1902:28	53.75 (53.75)	161.75 (161.85)	33	7
94/08/24 <sup>b</sup>	94/08/24 1517:40	-25.06 (-24.96)	-13.54 (-13.54)	10	1.4
94/10/25 <sup>c</sup>	94/10/25 0054:35	36.30	70.91	244	<sup>d</sup>
01/11/08 <sup>c</sup>	01/11/08 1742:55	-27.76	65.66	10	<sup>d</sup>
01/12/02 <sup>b</sup>	01/12/02 1301:54	39.40 (-39.20)	141.09 (141.29)	124	4

<sup>a</sup>Values in parentheses are relocated latitude, longitude and depth.

<sup>b</sup>Earthquake used as reference event for the additional correction for the S wave data.

<sup>c</sup>earthquake used as reference event for the additional correction for the P wave data.

<sup>d</sup>No earthquake relocation is applied to this event.

cate that the African Anomaly extends at least 1300 km above the CMB. In addition, *Masters et al.* [2000] reported an anticorrelation of bulk sound velocity perturbation and shear velocity perturbation in the deep mantle beneath Africa. The density anomalies associated with the African Anomaly in the mid-lower mantle are also studied. For example, *Ishii and Tromp* [1999] suggested that the low-velocity anomaly in the lower mantle beneath Africa has a higher density, while *Lithgow-Bertelloni and Silver* [1998] and *Gurnis et al.* [2000] argued that positive density buoyancy is needed in the mid-lower mantle in order to explain the high topography and the uplift rate observed in southern Africa. Possible origins of the African Anomaly in the mid-lower mantle include (1) a thermal mantle plume erupting off the top of the VLVP at the base of the mantle; (2) an unstable extension of the VLVP into the mid-lower mantle (i.e., it is compositionally distinct but unstable over geological time); and (3) a geologically stable VLVP extension into the mid-lower mantle. The geometry and the P and S velocity structure of the mid-lower mantle portion are of particular importance in distinguishing these possibilities. For example, a detached mid-lower mantle portion from the VLVP may more likely indicate that the mid-lower mantle portion represents a buoyant thermal plume erupting off the top of the VLVP, whereas a structurally connected one may indicate the anomaly in the mid-lower mantle has the same compositional origin as its base. An anomaly with both flanks in the mid-lower mantle dipping toward the same direction or with its lateral dimension decreasing with depth may indicate that the compositional anomaly is geologically unstable, whereas one with both flanks dipping toward its center may indicate the opposite [*Ni et al.*, 2002]. Also, of course, constraining both P and S velocity structure would be crucial to the understanding of the thermal and compositional origin of the anomaly. Recent seismic studies [*Ni et al.*, 1999, 2002; *Ni and Helmberger*, 2003a, 2003b, 2003c] proposed a ridge-like structure with both flanks of its upward extension in the lower mantle tilting toward northeast and a uniform shear velocity reduction of -3% with respect to PREM. However, these models were derived mostly by using seismic data sampling from the southwest-

ern direction, with few sampling from the opposite (north-eastern) direction. Now that the data sampling the anomaly from both directions are available, it is important to critically evaluate the geometry and the P and S velocities of the African Anomaly.

[4] In this paper, we constrain the geometry and P and S velocity structure of the African Anomaly along a great circle arc from the East Pacific Rise to the Japan Sea. We present seismic data and our modeling procedures in section 2, corrections for the effect of seismic heterogeneities outside the African Anomaly in section 3, and detailed constraints on the geometry and the P and S velocity structure in section 4. We then test other models and discuss the implications of seismic results in section 5.

## 2. Seismic Data and Modeling Procedures

### 2.1. Seismic Data

[5] We collect high-quality traveltimes and waveforms of direct S, ScS, SKS and SKKS phases to study the geometry and S wave velocity structure of the African Anomaly, and traveltimes of direct P and PcP phases to study the P wave velocity structure, from the recordings of earthquakes occurring in the East Pacific Rise (EPR), Drake Passage (DP), South Sandwich islands (SS), Iran (IR), Hindu Kush (HK), Xingjiang (XJ) and the Japan Sea (JS) (Figures 1a and 1b). We choose recordings for earthquakes with simple pulse-like source time functions for waveform modeling and travel time analysis. Our selected earthquakes include EPR97/06/10, DP95/01/03, SS95/03/26, SS97/09/05, SS97/10/05, SS02/02/10, SS02/03/09, IR98/03/14, HK97/05/13, XJ98/08/27 and JS97/12/05, coded by a combination of event location abbreviation and date (see event information in Table 1). The seismic data are selected from data recorded during the lifetimes of three broadband temporary PASSCAL seismic arrays in Africa: the Tanzania seismic array (1994–1995), the Kaapvaal seismic array (1997–1999) and the Ethiopia/Kenya seismic array (2000–2002). Our collected seismic data provide excellent sampling coverage in the lower mantle beneath southern Africa along the great arc from the East Pacific Rise to the Japan Sea

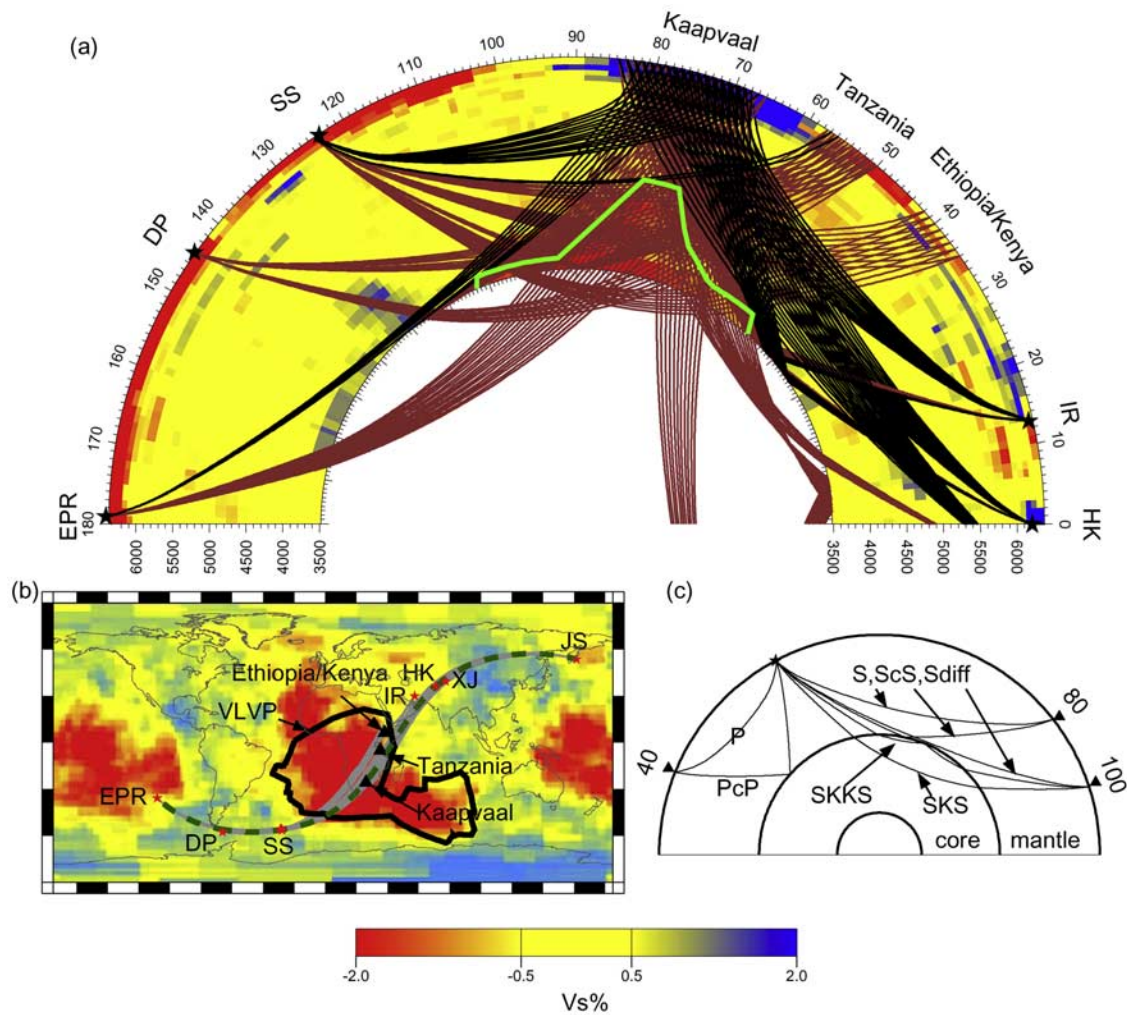


**Figure 1.** (a) Best fitting model (green contour) and raypaths of the seismic phases employed to constrain geometry and S velocity structure of the African Anomaly in a 2-D cross section along the East Pacific Rise (EPR), Drake Passage (DP), South Sandwich islands (SS), Iran (IR), and Hindu Kush (HK). Black and red traces represent propagation paths without and with observed traveltime delays that can be attributed to the African Anomaly, respectively. Note that the geometry of the African Anomaly in the lower mantle is confined below the paths with no traveltime delays (black traces). The best fitting model has average reductions of  $-5\%$  in shear velocity and  $-1.67\%$  in compressional wave velocity in the lowermost 250 km of the mantle and  $-2\%$  to  $-3\%$  in shear velocity and about  $-1\%$  in compressional wave velocity 150–250 km above the core-mantle boundary. Black stars represent seismic events. Seismic arrays and earthquake locations are denoted at the top of the Earth’s surface. The background are shear velocity perturbations from a global shear velocity tomographic model [Grand *et al.*, 1997]. (b) Map view of great circle paths (gray traces), locations of earthquakes (red stars) and seismic arrays (black triangles). The thick green dashed curve represents the 2-D cross section represented in Figure 1a, and the thick black contour is the geographic boundary of the VLVP at the base of the mantle [Wang and Wen, 2004]. Note that our collected seismic data sample the African Anomaly in a narrow azimuthal range of less than  $11^\circ$ . (c) Raypaths of direct S, ScS at  $80^\circ$ , P, PcP at  $40^\circ$ , and Sdiff, SKS, SKKS at  $100^\circ$ .

(Figure 1a). Note that all the seismic data sample the African Anomaly within a small azimuthal range of  $11^\circ$ . Seismic waves for the first seven events sample the African Anomaly from the southwestern direction, while those from the rest of the events sample the anomaly from the opposite (northeastern) direction (Figure 1b).

[6] All seismograms are deconvolved using their corresponding instrument responses and rotated to tangential, radial and vertical components. A band-pass filter with

a frequency range of 0.008–1 Hz is applied to all seismograms. The estimated uncertainty in time picks of the seismic phase onsets is 0.5–1 s.

## 2.2. Modeling Procedures

[7] Because the seismic data sample the African Anomaly within a small azimuthal range of  $11^\circ$  (Figure 1b), we use simplified two-dimensional (2-D) models in our forward

modeling procedure. Our traveltime forward modeling consists of four procedures:

[8] 1. We redetermine location and origin time of the chosen earthquakes using seismic observations recorded by the Global Seismographic Network (GSN) and a three-dimensional (3-D) shear velocity tomographic model [Grand *et al.*, 1997].

[9] 2. We correct for traveltime residuals that are caused by the mantle heterogeneities outside the African Anomaly; the corrections consist of predictions based on an S velocity tomographic model [Grand *et al.*, 1997] (for S waves) or a P velocity tomographic model [van der Hilst *et al.*, 1997] (for P waves) and an additional component associated with the underestimation of the 3-D tomographic models as discussed in section 3. The corrected traveltime residuals can be attributed to the African Anomaly.

[10] 3. We obtain the best fitting model by testing various geometries and shear velocity perturbations for the African Anomaly through trial and error forward modeling the observed shear wave travel time residuals. When the direct S, Sdiff, and ScS phases are involved, we calculate traveltime residuals with the SH hybrid method [Wen, 2002].

[11] 4. We search for the best fitting S to P velocity perturbation ratio by testing various uniform S and P velocity perturbation ratios using the geometry and shear velocity structure of the African Anomaly determined from the first three procedures.

[12] Details of the event relocation procedure can be found in Appendix A1; results from other procedures are presented in the subsequent sections.

### 3. Traveltime Corrections for the Effect of Seismic Heterogeneities Outside the African Anomaly

[13] Our corrections for the traveltime perturbations caused by the seismic heterogeneities outside the African Anomaly consist of two components. One component is the predicted traveltime delays caused by the seismic heterogeneities outside the African Anomaly based on a global tomographic shear (for S waves) or compressional (for P waves) velocity model; the other component is an additional correction for the traveltime variations that are underestimated in the global tomography models. The first procedure is straightforward. We set the velocity perturbations in the African Anomaly to be zero in the global tomographic models and calculate the traveltime perturbations based on the modified tomographic models and the raypaths associated with the actual event and station locations. We explain the necessity and procedure of the additional corrections in the following paragraphs.

[14] The Kaapvaal, Tanzania and Ethiopia/Kenya seismic arrays were deployed over complex geological settings from the Archean cratons in southern Africa to the extensional Ethiopian rift region in eastern Africa. Strong lateral seismic anomalies underlie those three arrays. We show three examples for three events whose S waves propagate outside the African Anomaly in Figure 2. Large traveltime residuals are observed across the arrays (Figure 2a for the Kaapvaal seismic array, Figure 2d for the Tanzania seismic array, and Figure 2g for the Ethiopia/Kenya seismic array), suggesting that the traveltime residuals associated with the three-

dimensional seismic structure outside the African Anomaly are large and corrections are required before one can attribute the traveltime residuals to the African Anomaly. The predicted traveltime residuals based on a global shear velocity tomographic model by Grand *et al.* [1997] exhibit similar patterns to those of the observed traveltime residuals across seismic arrays (middle panels) and can account for a large fraction of the observed traveltime delays, but they cannot fully account for the magnitude (Figures 2b, 2e, and 2h) and small-scale traveltime delay variations observed within the seismic arrays (Figure 2, right). The observed P traveltime variations associated with three-dimensional seismic structure are large across the arrays (Figure 3a), and the global compressional tomography model we employed [van der Hilst *et al.*, 1997] also underestimates both the magnitude and the small-scale variations of the travel time residuals. This is understandable because the dense observations of the seismic arrays are not built into as constraints on these global seismic tomography models. Therefore it is necessary to make additional traveltime corrections for the effect of the seismic heterogeneities beneath the seismic arrays.

[15] To calculate the additional S traveltime corrections for each array, we choose an event whose S waves propagate outside the African Anomaly as a reference event so that the additional travel time corrections do not remove any signals associated with the African Anomaly. The additional correction at each station is the difference of the traveltime residual observed for the reference event and the prediction based on Grand *et al.*'s [1997] model for the reference event. We use event SS97/09/05, a seismic event occurring in the South Atlantic Ocean (event 94/08/24) and an earthquake in the Japan Sea (event 01/12/02) as reference events for the Kaapvaal, Tanzania and Ethiopia/Kenya seismic arrays, respectively (see event locations and great circle paths in the lower corners of Figures 2a, 2d, and 2g). The seismic phases used for the S wave traveltime correction are direct S phases for the Kaapvaal and Tanzania seismic arrays and SKS phases for the Ethiopia/Kenya seismic array. The patterns of the additional traveltime corrections strongly correlate with the geological setting in these three arrays (Figures 2c, 2f, and 2i). For example, the additional corrections for the Kaapvaal seismic array have zero values for those of the in-craton stations and positive values for those of the stations beneath the Cape Fold belt and the Namaqua-Natal mobile belt (Figure 2c).

[16] To calculate the additional P traveltime corrections for each array, we choose an event whose P waves propagate outside the African Anomaly as a reference event and some stations as reference stations. The additional correction at each station is the difference of the traveltime residual observed for the reference event and the prediction based on van der Hilst *et al.*'s [1997] model for the reference event. We use event SS97/10/05 as reference event and the in-craton stations as reference stations for the Kaapvaal seismic array, a seismic event occurring in Hindu Kush (event 94/10/25) as reference event and GSN stations BOSA, LSZ, TSUM as reference stations for the Tanzania seismic array, and an earthquake in the South Indian Ocean (event 01/11/08) as reference event and GSN stations BOSA and TSUM as reference stations for the Ethiopia/Kenya seismic array. The patterns of the additional

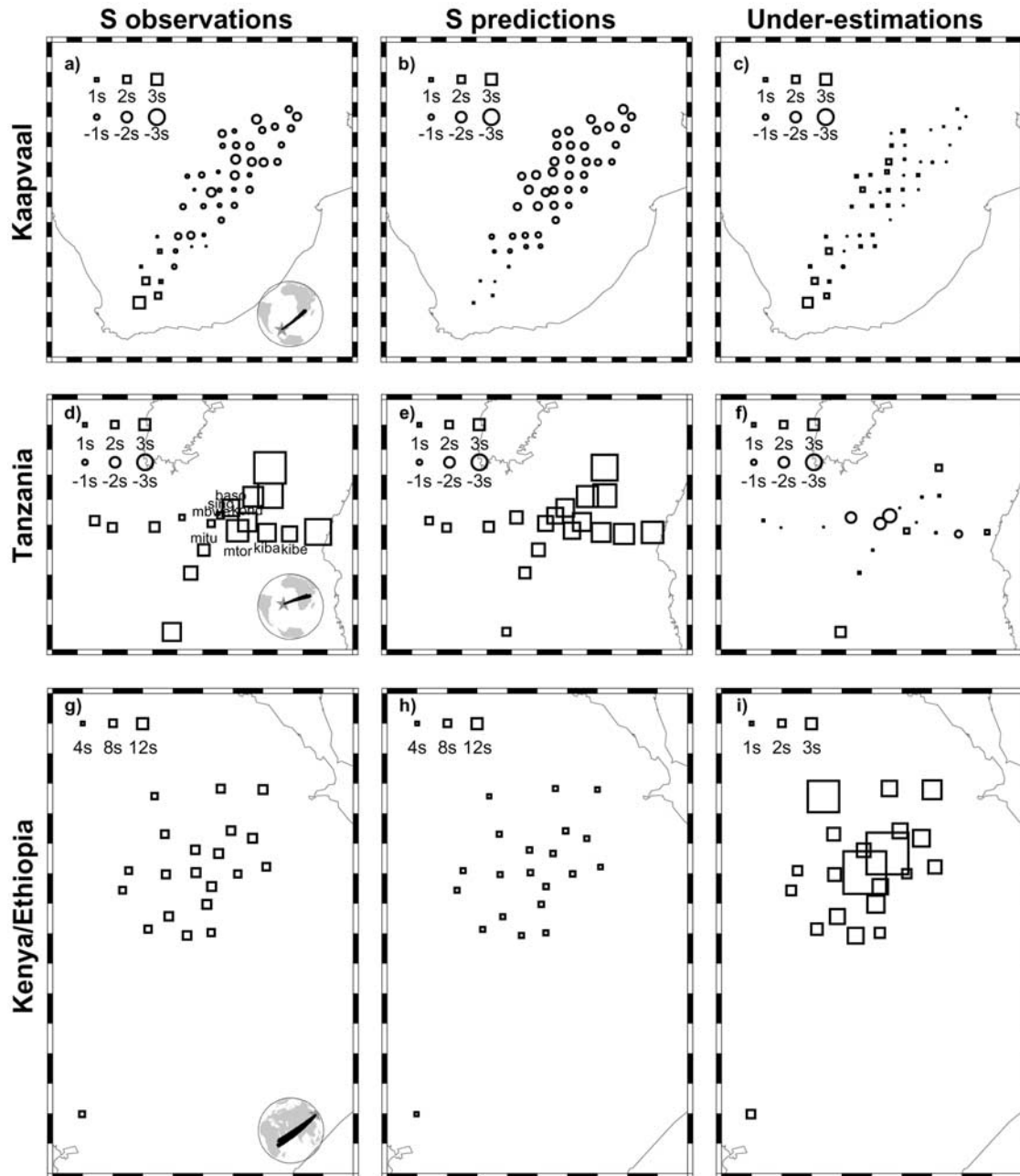


**Figure 2.** (a, d, g) Observed direct S or SKS traveltime residuals for reference events, (b, e, h) predicted S traveltime residuals for reference events based on *Grand et al.*'s [1997] model and (c, f, i) observed S traveltime residuals for the reference events after corrected for the effects due to the seismic heterogeneities outside the African Anomaly based on *Grand et al.*'s [1997] model. Note that the direct S or SKS phases for the reference events propagate outside the African Anomaly. All these traveltime residuals are plotted with respect to the predictions based on PREM and at the locations of each seismic stations for the Kaapvaal (Figures 2a, 2b, and 2c), Tanzania (Figures 2d, 2e, and 2f) and Ethiopia/Kenya (Figures 2g, 2h, and 2i) seismic arrays. Figures 2c, 2f, and 2i show second component of the S traveltime correction. The additional corrections in Figures 2c, 2f, and 2i are obtained by subtracting the traveltime residuals predicted based on *Grand et al.*'s [1997] model (Figures 2b, 2e, and 2h) from those observed (Figures 2a, 2d, and 2g). The great circle paths, event location of the reference event, and station location are plotted in the bottom right corner of Figures 2a, 2d, and 2g. Squares and circles denote positive and negative traveltime delays, respectively, with their sizes proportional to the magnitudes of traveltime delay.

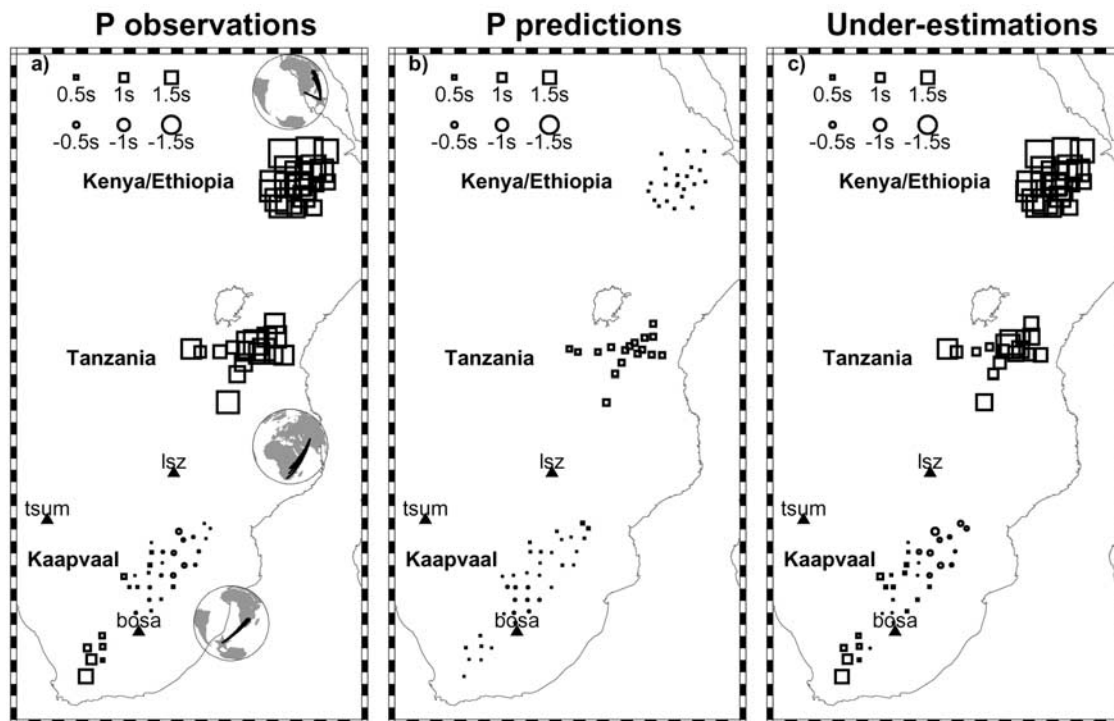


**Figure 3.** (a) Observed direct P traveltime residuals for reference events, (b) predicted P traveltime residuals for reference events based on *van der Hilst et al.*'s [1997] model and (c) the P traveltime residuals for the reference events after corrected for the effects due to the seismic heterogeneities outside the African Anomaly based on a global compressional velocity tomographic model [*van der Hilst et al.*, 1997]. Note that the direct P phases for the reference events propagate outside the African Anomaly. All these traveltime residuals are calculated with respect to the predictions based on PREM and the observed residuals at the reference stations. They are plotted at the locations of each seismic station for the Kaapvaal, Tanzania, and Ethiopia/Kenya seismic arrays. Figure 3c shows the second component of the P traveltime correction. The additional corrections in Figure 3c are obtained by subtracting the traveltime residuals predicted based on *van der Hilst et al.*'s [1997] model (Figure 3b) from those observed (Figure 3a). The great circle paths, location of the reference event, and station location are plotted near the seismic arrays. Squares and circles denote positive and negative traveltime delays, respectively, with their sizes proportional to the magnitudes of traveltime delay.

P traveltime corrections also strongly correlate with the geological setting in these three arrays (Figure 3, right).

[17] For each seismic observation, the total traveltime correction for the seismic heterogeneities outside the African Anomaly are the summation of the additional corrections associated with the stations in Figures 2c, 2f, and 2i (for S waves) or Figure 3c (for P waves) and the predicted traveltime residuals based on *Grand et al.*'s [1997] (for S waves) or *van der Hilst et al.*'s [1997] (for P waves) models (with zero contribution from the African Anomaly) and actual event and station locations.

#### 4. Geometry and P and S Velocity Structure of the African Anomaly

[18] In this section, we first present results of the geometry and shear velocity structure of the African Anomaly based on waveform modeling and traveltime analysis of the observations for the seismic phases sampling the anomaly from the southwestern and the northeastern directions. We then discuss in detail the compressional velocity structure of

the African Anomaly based on traveltime analysis of the P wave data. As no noticeable travel time difference is found between the SH and SV direct arrivals for the seismic data sampling the base [*Fouch et al.*, 1999; *Wen*, 2002], we therefore neglect the influence of anisotropy in the lower mantle beneath southern Africa. Note that all the data presented in this section have been corrected for the mislocation of the earthquakes and the effects of seismic heterogeneities outside the African Anomaly, i.e., after procedures 1 and 2. They can only be attributed to the African Anomaly.

#### 4.1. Geometry and S Velocity Structure

##### 4.1.1. Depth Extent of the Anomaly

[19] The direct S traveltime residuals observed for two events occurring in South Sandwich islands: SS97/09/05 and SS95/03/26 place tight constraints on the depth extent of the African Anomaly (Figure 1a). The direct S phases show no traveltime delay between  $44^\circ$  and  $69^\circ$  for events SS97/09/05 and SS95/03/26, and gradually increasing traveltime delays from about 0 s at  $69^\circ$  to 3 s at  $74^\circ$  for event

## SS97/09/05 and SS95/03/26

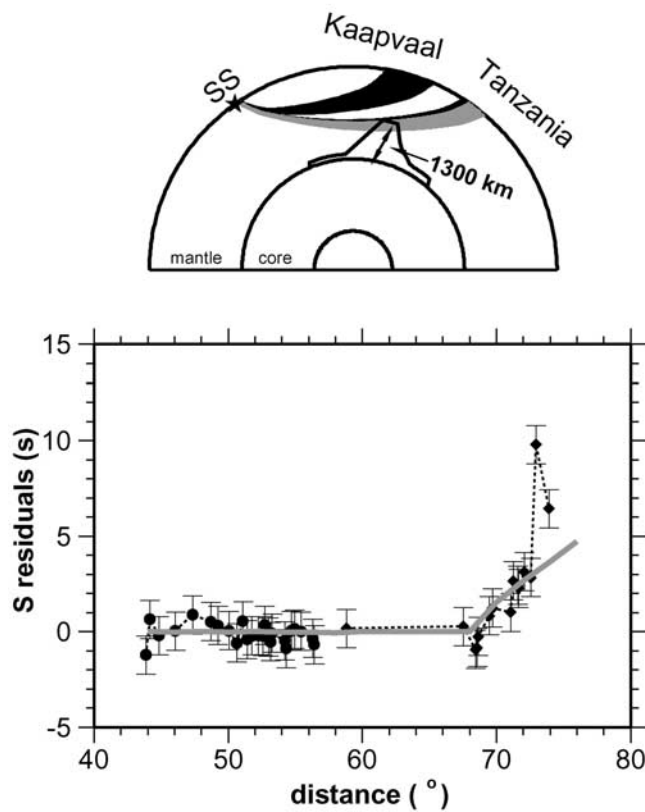


**Figure 4.** (bottom) Observed direct S traveltimes residuals with respect to PREM for events SS97/09/05 (black dots) and SS95/03/26 (black diamonds) and predictions (gray curve) from the 2-D SH hybrid method waveform modeling results for the best fitting model. (top) Corresponding direct S raypaths with respect to the location of the best fitting model, with the paths of no traveltimes delays shown in heavy shading. The error bars in traveltimes pick of 1 s are also shown.

SS95/03/26 (Figure 4). The bottoming depths of these direct S waves are about 1520–1860 km and 940–1170 km above the CMB for events SS97/09/05 and SS95/03/26, respectively. Therefore the African Anomaly must extend at least 1300 km above the CMB to account for the S wave traveltimes delays observed after 69° (Figure 4). The fact that no traveltimes delays are observed before 69° indicates that the depth extent of the African Anomaly is well constrained. There is no evidence that the anomaly extends farther into the shallower part of the mantle sampled by these direct S waves.

### 4.1.2. Southwestern Side

[20] The southwestern flank of the African Anomaly is constrained by Sdiff and SKS phases from event EPR97/06/10, direct S phase from event DP95/01/03, and direct S and ScS phases from events SS97/09/05, SS95/03/26 and SS02/02/10 (see Figure 1a). The Sdiff phase observed for event EPR97/06/10 exhibits simple pulse-like waveforms and no traveltimes delay with respect to the predictions based on

PREM at distances less than 103° (Figures 1a and 5a), placing tight constraints on the geographic extent of the southwestern flank of the anomaly. After 103°, the Sdiff phase shows linearly increasing traveltimes delays of up to 8 s at 113°. These linearly increasing traveltimes delays are likely caused by seismic heterogeneities in the receiver-side lower mantle, as other possible factors can be confidently ruled out: (1) they cannot be attributed to mislocation of the earthquake as earthquake mislocation would yield a uniform, rather than a linearly increasing, time shift across the array; (2) they are not due to the seismic heterogeneities in the source-side mantle as the propagation paths of these Sdiff waves are nearly identical there (see Figure 1a); and (3) they are not caused by the seismic heterogeneities in the receiver-side upper mantle or crust, as the direct S waves recorded at close distances along the same azimuth that have similar near-station raypaths (such as those for event SS97/09/05) do not show traveltimes delays across the array. However, based on the Sdiff traveltimes alone, it is impossible to pin down which portion of the receiver-side lower mantle contributes those traveltimes delays, as both a basal low-velocity layer and a gradual increase of vertical extent of the anomaly would explain the traveltimes delays equally well. The traveltimes delays observed for the SKS phase from the same event and the direct S phase from event DP95/01/03, as well as the ScS–S differential traveltimes observed for events SS97/09/05 and SS95/03/26, suggest that the southwestern flank of the anomaly is northeast of the Sdiff propagation paths in the mid-lower mantle (Figure 5c). Therefore the observed Sdiff traveltimes delays and waveforms between 103° and 113° are caused by a basal low-velocity layer at the base of the mantle. These observed traveltimes delays can be well explained by a 200-km-thick basal low-velocity layer in the lowermost mantle. Note that, a 200-km-thick basal layer at the base of the mantle that is located about 7000 km laterally away from the event location and has a strong linear shear velocity reduction gradient from –2% (top) to –12% (bottom), can well predict the onset distance of the traveltimes delays (103°) and the linearly increasing traveltimes delays after 103° observed in the data (Figure 5b). We adopt a linear gradient of shear velocity decrease obtained from our previous studies in this area [Wen *et al.*, 2001; Wang and Wen, 2004]. The slope of the Sdiff residuals and its onset distance are controlled by model thickness, edge dip, and lateral location of the basal layer. Synthetic tests indicate that model uncertainties are about 50–100 km in thickness and about 500 km in lateral location.

[21] SKS traveltimes residuals for event EPR97/06/10 are about 1–2 s at distances less than 101°, linearly increase to 6.7 s at 107° and remain at about 4–6 s at distances between 107° and 113° (Figure 5d). The observed relatively small and uniform SKS traveltimes residuals at distances less than 101° suggest that the southwestern flank of the anomaly in the mid-lower mantle is northeast of the Sdiff raypaths for event EPR97/06/10. The observed SKS traveltimes delays at distances less than 101° are consistent with a model that SKS phases propagate through a relatively uniform basal layer as inferred from the waveform modeling of the Sdiff phases (Figure 5c). At distances between 101° and 107°, SKS phases pass through the southwestern flank of the anomaly in the mid-lower mantle and generate a rapid

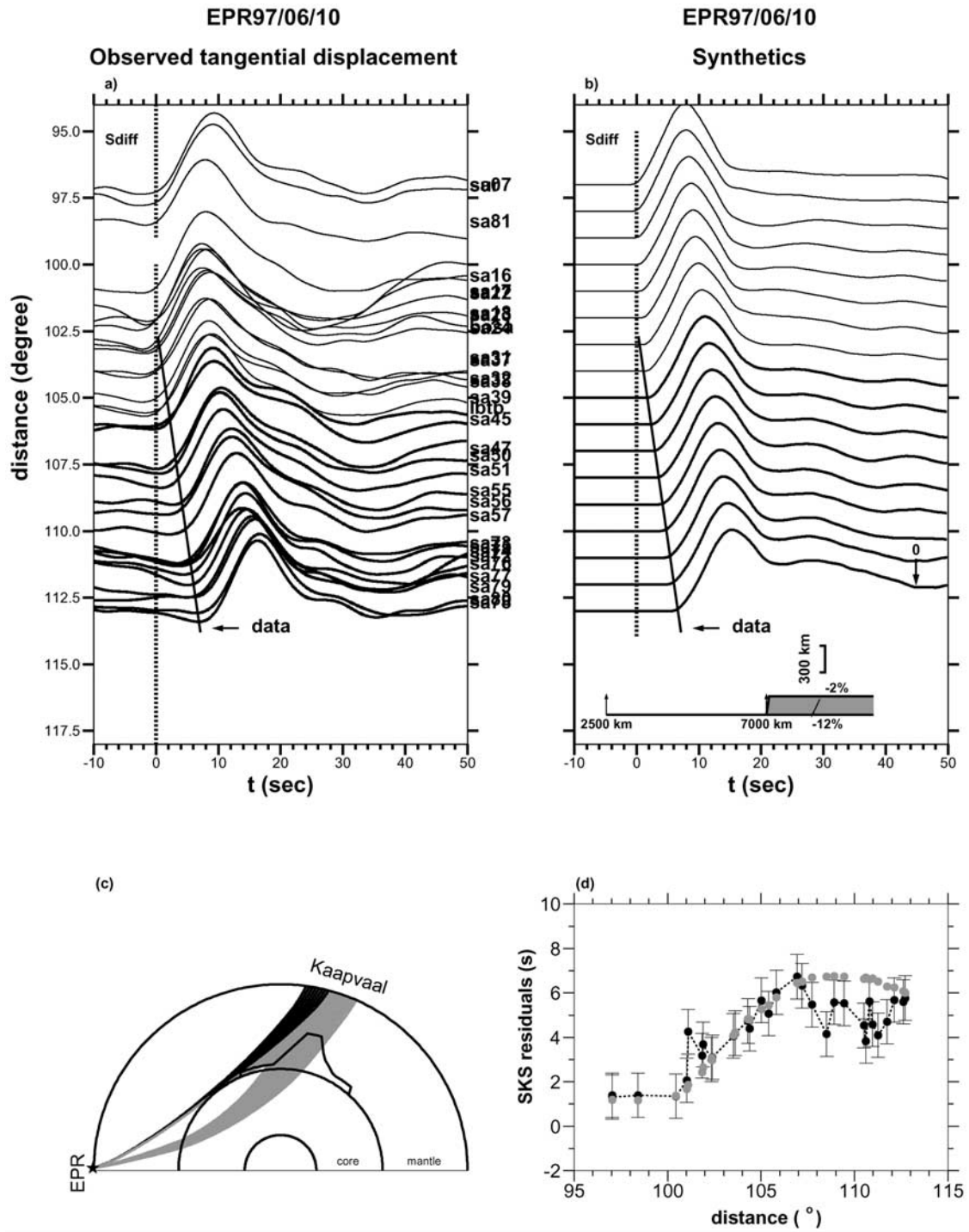


**Figure 5.** (a) Observed tangential displacements for event EPR97/06/10 and (b) synthetics calculated with the 2-D SH hybrid method for a 200-km-thick basal layer at the bottom of the mantle with a linear decrease of shear velocity from  $-2\%$  (top) to  $-12\%$  (bottom) with respect to PREM (see model in Figure 5c). Also labeled in the model are the horizontal distances from the earthquake source. The observed Sdiff recordings and synthetics are aligned along predicted Sdiff arrivals based on PREM. The black line indicates the slope of observed traveltime variations for the recordings at distances greater than  $103^\circ$ . The phase labeled 0 in Figure 5b is a truncation phase of the SH hybrid method calculation. (c) Sdiff and SKS raypaths with respect to the location of the best fitting model, with the paths of no traveltime delays shown in heavy shading, and (d) observed SKS traveltime residuals (black dots) for event EPR97/06/10 with respect to PREM and predicted SKS residuals (gray dots) from forward traveltime modeling based on our best fitting model (Figure 1a). Shown also are the error bars in traveltime pick.

## DP95/01/03

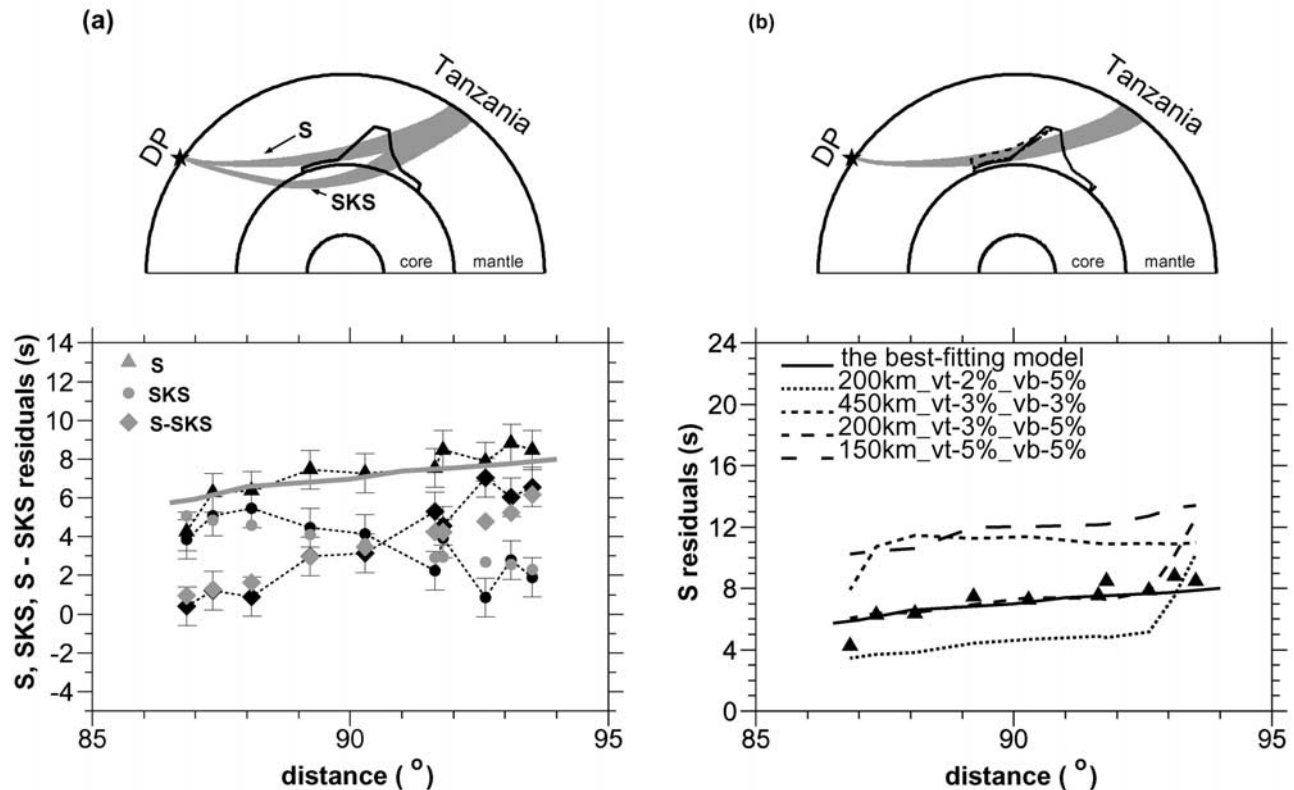


**Figure 6.** (a) (bottom) Observed direct S (black triangles), SKS (black dots), S-SKS differential (black diamonds) traveltime residuals with respect to PREM for event DP95/01/03 and predicted direct S (gray curve) from the 2-D SH hybrid method waveform modeling results, SKS (gray dots) and S-SKS differential (gray diamonds) traveltime residuals from the forward traveltime modeling results based on our best fitting model. (top) Corresponding S and SKS raypaths with respect to the location of the best fitting model. Shown also are the error bars in the traveltime picks. (b) (bottom) Comparison of observed direct S traveltime residuals (black triangles) for event DP95/01/03 and predictions based on our best fitting model (solid curve) and four other models (dashed curves) perturbed from the best fitting model with different thickness for the southwestern base of the anomaly and different shear velocity reductions. The perturbed models include those with a thickness of 200 km in the base and a shear velocity reduction of  $-2\%$  in the mid-lower mantle portion (200km\_vt-2%\_vb-5%), with a thickness of 450 km in the base and a uniform shear velocity reduction of  $-3\%$  in both portions (450km\_vt-3%\_vb-3%), with a thickness of 200 km in the base and a shear velocity reduction of  $-3\%$  in the mid-lower mantle portion (200km\_vt-3%\_vb-5%), and with a thickness of 150 km in the base and a uniform shear velocity reduction of  $-5\%$  in both portions (150km\_vt-5%\_vb-5%). (top) Corresponding direct S raypaths with respect to the locations of the best fitting model and the perturbed models.

increase of traveltime delays of up to 6.7 s. SKS propagation paths cross over the apex of the anomaly at about  $107^\circ$  and start to sample the northeastern flank of the anomaly at the larger distances, producing slightly decreasing traveltime delays at distances greater than  $107^\circ$ . The observed rapid increase of SKS traveltime delays from  $101^\circ$  to  $107^\circ$  places tight constraints on the lateral location of the southwestern flank of the anomaly. The lateral location of the southwestern flank of the anomaly has an uncertainty of about 200 km. The magnitude of the observed SKS traveltime residuals around  $107^\circ$  is controlled by the average shear velocity reduction and the height of the anomaly. With

the thickness of the basal layer well constrained by the Sdiff waveforms and the height of the anomaly by the S traveltime residuals from events SS97/09/05 and SS95/03/26, the geometry of the southwestern flank is well constrained.

[22] The southwestern flank of the African Anomaly is also sampled by direct S phases from event DP95/01/03. The observed S traveltime residuals linearly increase from 4 s at  $87^\circ$  to about 8 s at  $93^\circ$ , while the SKS traveltime residuals decrease from 5 s to 2 s over the same distance range (Figure 6a). The differential S-SKS traveltime residuals show an increase from  $-1$  s at  $87^\circ$  to 6 s at  $94^\circ$ . As the SKS phases for this event sample the northeastern side of

## SS97/09/05 and SS95/03/26

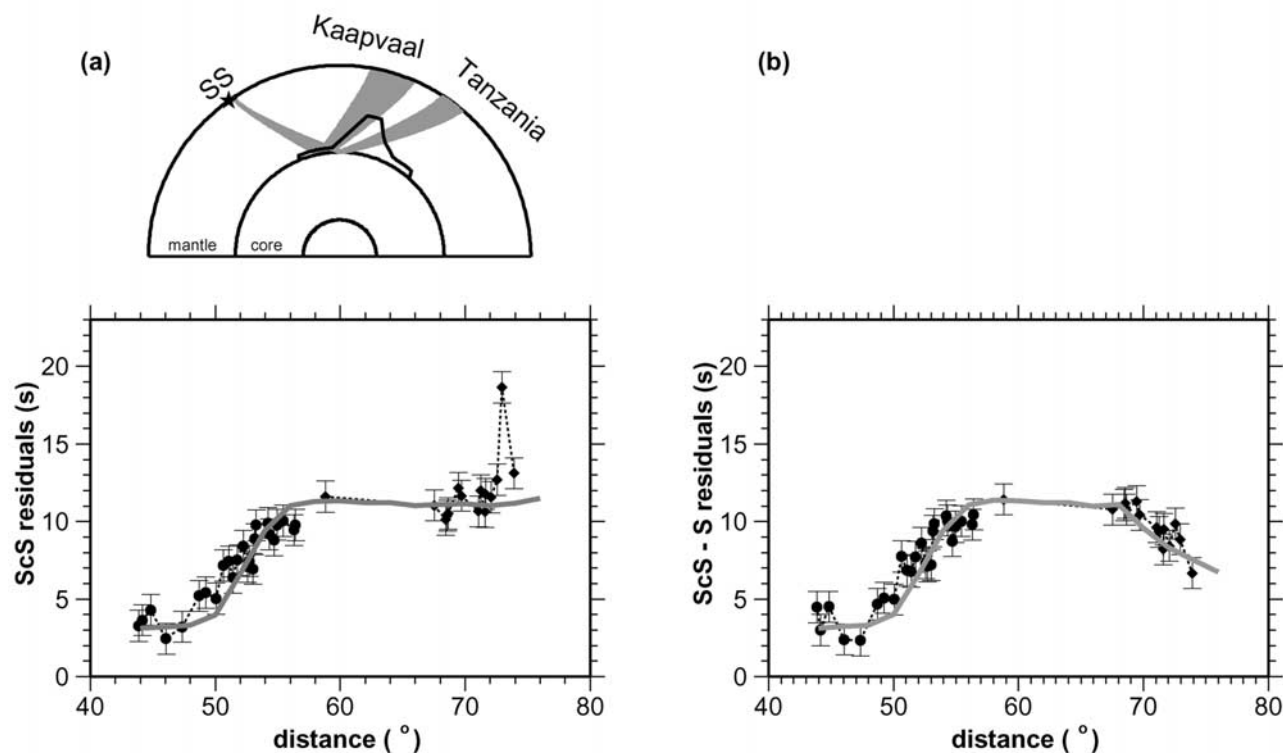


**Figure 7.** (a) (bottom) Observed ScS traveltime residuals for events SS97/09/05 (black dots) and SS95/03/26 (black diamonds) with respect to PREM and predictions (gray curve) from the 2-D SH hybrid method waveform modeling results based on the best fitting model. (top) Corresponding ScS raypaths with respect to the location of the best fitting model. (b) Observed ScS-S traveltime residuals with respect to PREM for events SS97/09/05 (black dots) and SS95/03/26 (black diamonds) and predictions (gray curve) from the 2-D SH hybrid method waveform modeling results based on the best fitting model. Shown also in Figures 7a and 7b are the error bars in traveltime pick.

the African Anomaly, we discuss them later. The bottoming depths for the direct S phases range from 150 km to 1000 km above the CMB (Figure 1a). The gradually increasing direct S traveltime residuals indicate that the southwestern flank of the African Anomaly extends from 150 km above the CMB to at least 1000 km above the CMB. Those traveltime residuals further constrain the thickness of the basal layer to be 150 km and average shear velocity reduction to be about  $-3\%$  for the portion of the anomaly in the mid-lower mantle. A basal layer with a thickness exceeding 150 km for the southwestern base of the African Anomaly would predict an abrupt increase of traveltime delay in the distance range from  $85^\circ$  to  $94^\circ$ , different from the observed S traveltime pattern in the data. For example, basal layers with thicknesses of 200 km and 450 km predict a kink in traveltime delay at about  $92^\circ$  and  $88^\circ$ , respectively (Figure 6b). The shear velocity perturbation for the portion of the African Anomaly in the mid-lower mantle is well constrained by the magnitudes of the observed traveltime delays. An average shear velocity reduction of  $-2\%$  would underpredict S traveltime residuals in the whole distance range by 2–3 s, whereas an average shear velocity reduction of  $-5\%$  overpredicts S traveltime residuals by about 4 s

(Figure 6b). Waveform modeling of the Sdiff phases for event EPR97/06/10 suggests a thickness of 200 km in the southwestern base. This difference is within the uncertainties of the thickness estimate. It may also be explained by the fact that those phases sample different portions of the basal layer and a lateral variation in thickness may exist across the basal layer. Overall, predictions based on our best fitting model match well both the general trend and magnitude of direct S residuals observed in the whole distance range (Figure 6a).

[23] The ScS-S differential traveltime residuals observed for events SS97/09/05 and SS95/03/26, and direct S traveltime residuals for event SS02/02/10 place further constraints on the geometry and shear velocity structure on the southwestern side of the African Anomaly. The observed ScS traveltime residuals increase from about 3 s at  $44^\circ$  to 10 s at  $57^\circ$  for event SS97/09/05, and remain at about 10 s at distances between  $68^\circ$  and  $74^\circ$  for event SS95/03/26 (Figure 7a). The ScS-S differential traveltime residuals increase rapidly at about  $48^\circ$  when the ScS phases for event SS97/09/05 start sampling the portion of the anomaly in the mid-lower mantle (Figure 7b). An average shear velocity reduction of about  $-5\%$  in the base is required to match the

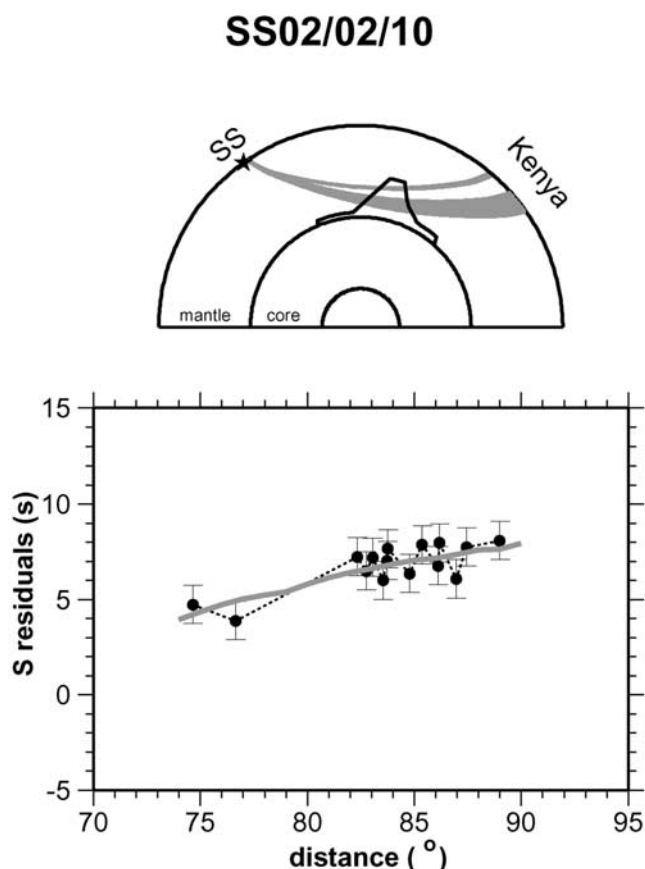


**Figure 8.** (bottom) Observed direct S travel time residuals (black dots) with respect to PREM for event SS02/02/10 and predictions (gray curve) from the 2-D SH hybrid method waveform modeling results based on the best fitting model. (top) Corresponding direct S raypaths with respect to the location of the best fitting model. Shown also are the error bars in traveltimes pick.

ScS-S differential travel times observed before  $48^\circ$  (Figure 7b). *Simmons and Grand* [2002] also used the ScS-S and PcP-P differential traveltimes for event SS97/09/05 to study the seismic structure near the CMB. They obtained a shear velocity reduction of  $-9\%$  for a 150-km-thick layer or a shear velocity reduction of  $-5\%$  for a 300-km-thick layer. Because they assumed no contribution from the portion of the anomaly in the mid-lower mantle, their shear velocity perturbations are expected to be larger than ours. With the thickness well constrained by the Sdiff waveform for event EPR97/06/10 (Figures 5a and 5b) and the direct S traveltime residuals for event DP95/01/03 (Figure 6b), the ScS-S differential traveltimes are used as another independent constraint on shear velocity reduction of the base. A shear velocity reduction of less than  $-5\%$  would underpredict ScS-S differential traveltimes observed for event SS95/03/26. The direct S phases for event SS02/02/10 show gradually increasing traveltime delays from about 3 s at  $74^\circ$  to 8 s at  $90^\circ$  (Figure 8). These direct S phases sample the middle of the anomaly and their traveltimes place constraints on the magnitude of shear velocity reduction in the middle of the African Anomaly to be  $-3\%$ .

[24] In short, our seismic data show that a 150- to 200-km-thick base on the southwestern side of the African Anomaly extends farther southwest and the African Anomaly regionally extends from the CMB to 1300 km above the CMB into the lower mantle beneath southern Africa with its southwestern edge dipping toward its apex. The average shear velocity reduction is about  $-5\%$  in the base and  $-3\%$  in the mid-lower mantle.

#### 4.1.3. Northwestern Side

[25] The northeastern flank of the African Anomaly is sampled by direct S, ScS and SKS phases from events IR98/03/14, HK97/05/13 and XJ98/08/27, SKS phases from event DP95/01/03, and SKS and SKKS phases from event JS97/12/05 (Figure 1a). The direct S phases observed for event HK97/05/13 do not exhibit any significant traveltime delays from  $67^\circ$  to  $83^\circ$  (Figure 9a), nor do the ScS phases for the same event before  $78^\circ$  (Figure 9b). The direct S waves for events IR98/03/14 and XJ98/08/27, which sample similar upper mantle region beneath southern Africa but different part of the lower mantle (Figure 1a), also show no traveltime delays (Figures 10a and 11). The direct S and ScS propagation paths with no observed traveltime delay place tight bounds on the geographic extent of the African Anomaly on the northeastern side. The ScS waves for event IR98/03/14 show no traveltime delays before  $61^\circ$ , but a trend of increasing traveltime delays of up to 4 s at distances from  $61^\circ$  to  $72^\circ$  (Figure 10b). A similar ScS traveltime pattern is observed for event HK97/05/13, with the trend of increasing delays observed at distances greater than  $78^\circ$ . These ScS travel time delays are caused by a basal layer in the lowermost mantle. They place bounds on the geographic extent of the anomaly both at the CMB and in the mid-lower mantle on the northeastern side. The SKS phases for event XJ98/08/27 further constrain and confirm the inferred geometry and shear velocity structure of the northeastern flank of the anomaly. The SKS waves show traveltime delays of about 5–8 s between  $85^\circ$  and  $92^\circ$  (Figure 11). Such large traveltime delays would require that the SKS waves sample a large vertical extent of the anomaly along their ray paths.

[26] SKS and SKKS phases recorded for event JS97/12/05 place tight constraints on the geometry and shear velocity structure of the northeastern flank of the anomaly. SKS phases show uniform travel time delays of about 2.2 s before  $132^\circ$ , linearly increasing delays from about 2.2 s at  $132^\circ$  to up to about 4.8 s at  $137^\circ$ , and uniform delays of about 4.8 s after  $137^\circ$  (Figure 12a). The exit points of the SKS phases at the CMB are between those of the SKS phases for event DP95/01/03 and the bouncing points at the CMB of the ScS phases for event HK97/05/13. The observed large, but relatively uniform, travel time residuals at the distances before  $132^\circ$  confirm the existence of a basal layer with a large velocity reduction extending farther northeast, as suggested by the ScS traveltime residuals observed at the large distances for events IR98/03/14 and HK97/05/13 (Figures 9b and 10b). The observed pattern of the SKS traveltime residuals for event JS97/12/05 is similar to that of the SKS phases for event EPR97/06/10 sampling the southwestern flank of the anomaly, except in a reverse direction. Combined with the constraints provided by the nondelayed direct S and ScS phases for events IR98/03/14, HK97/05/13 and XJ98/08/27, the linear increase of the SKS

## HK97/05/13

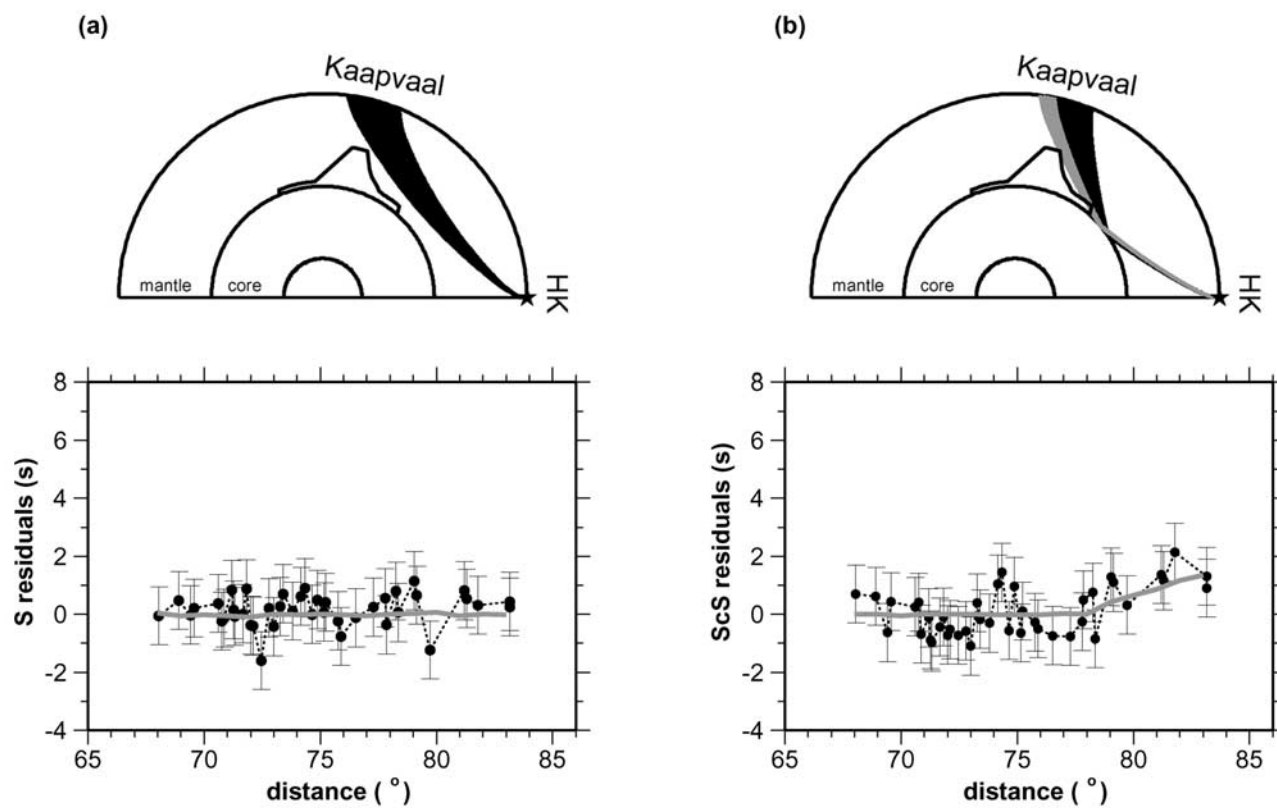


**Figure 9.** (a) (bottom) Observed direct S traveltime residuals (black dots) with respect to PREM for event HK97/05/13 and predictions (gray curve) from the 2-D SH hybrid method waveform modeling results based on the best fitting model. (top) Corresponding direct S raypaths with respect to the location of the best fitting model, with the paths of no traveltime delays shown in a heavy color. (b) Same as Figure 9a, except for the ScS phases of the same event. Shown also in Figures 9a and 9b are the error bars in travel time pick.

traveltime residuals for event JS97/12/05 at distances from  $129^\circ$  to  $137^\circ$  indicates that the northeastern flank of the anomaly also dips toward its center. SKKS phases for event JS97/12/05 exhibit relatively uniform delays of about 2.5 s at distances smaller than  $140^\circ$  and rapidly increasing delays to about 4 s at  $145^\circ$  (Figure 12b). This observed traveltime pattern is in agreement with the inferred geometry in the northeastern side of the anomaly. The SKKS phases sample the basal layer before  $140^\circ$  and the northeastern flank of the anomaly beyond  $140^\circ$ . The SKKS sampling paths are geographically the same as those of the SKS phases for event XJ98/08/27 (Figure 1a). The SKS traveltime residuals before  $132^\circ$  and the SKKS travel time residuals before  $140^\circ$  place tight constraints on the seismic velocity reduction at the base to be  $-5\%$ , with the thickness of the basal layer bounded by the observations from the nondelayed direct S and ScS phases from events IR98/03/14, HK97/05/13 and XJ98/08/27. With the top of the African Anomaly well bounded from the direct S wave traveltimes observed for event SS95/03/26, SKS traveltime residuals after  $132^\circ$  and SKKS traveltime residuals after  $140^\circ$  for event JS97/12/05 place constraints on the velocity reduction in the mid-lower

mantle portion to be about  $-2\%$ . The observed SKS and SKKS traveltime residuals can be well explained by our best fitting model with the northeastern edge dipping toward its center and average shear velocity reductions of  $-5\%$  in a 250-km-thick base and of  $-2\%$  in the portion above the base (Figures 12a and 12b).

[27] SKS and SKKS traveltime residuals recorded for event JS97/12/05 are sensitive to seismic velocity structure in the mid-lower mantle and at the base of the mantle. We present examples of comparisons between the observations and predictions based on several seismic velocity models perturbed from the best fitting model, including a shear velocity decrease of  $-3\%$  in the portion in the mid-lower mantle with a shear velocity decrease of  $-5\%$  in the base, and a shear velocity decrease of  $-1\%$  in the mid-lower mantle portion with a shear velocity decrease of  $-6\%$  in the base, and a uniform shear velocity decrease of  $-3\%$  (Figures 13a and 13b). A velocity reduction smaller than  $-5\%$  in the basal layer underpredicts SKS traveltime delays between  $130^\circ$  and  $135^\circ$  and SKKS traveltime delays between  $130^\circ$  and  $140^\circ$  (for example, model 250km\_vt-3%\_vb-3%), Figures 13a and 13b), while a velocity reduc-

## IR98/03/14

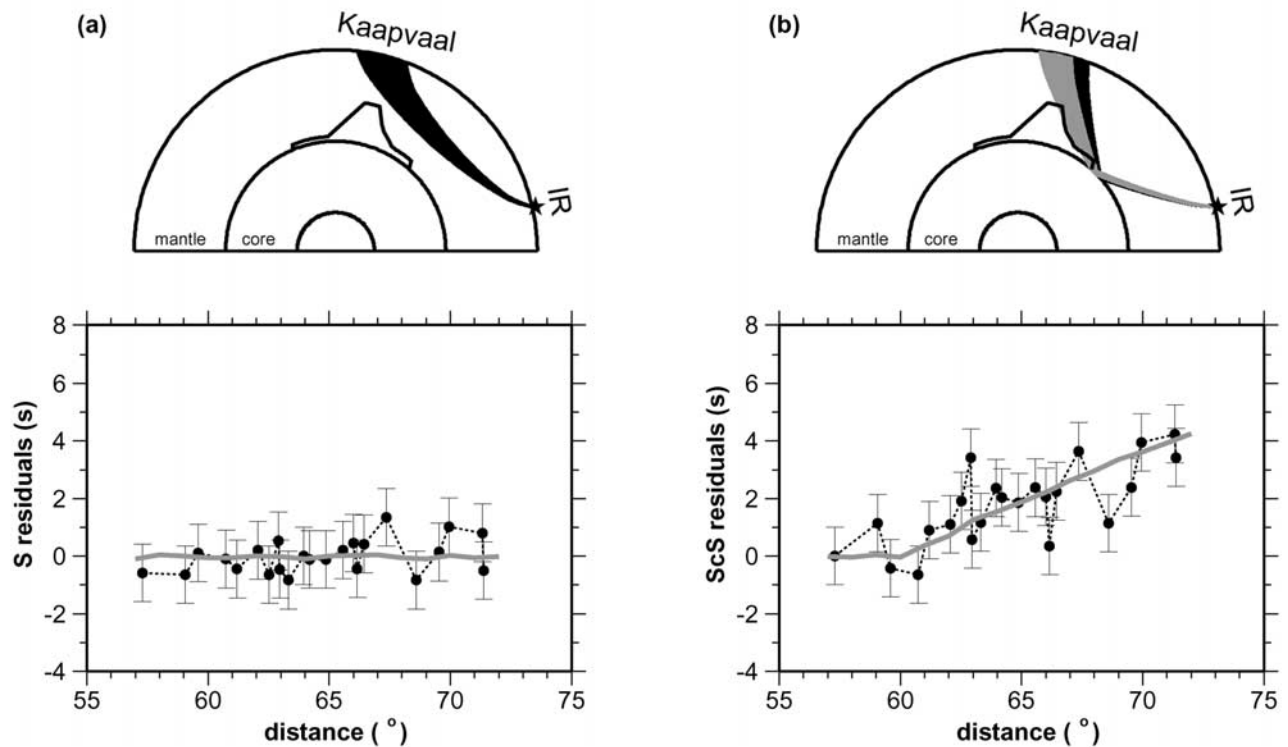


**Figure 10.** (a) (bottom) Observed direct S traveltime residuals (black dots) with respect to PREM for event IR98/03/14 and predictions (gray curve) from the 2-D SH hybrid method waveform modeling results based on the best fitting model. (top) Corresponding direct S raypaths with respect to the location of the best fitting model, with the paths of no traveltime delays shown in a heavy color. (b) Same as Figure 10a, except for the ScS phases of the same event. Shown also in Figures 10a and 10b are the error bars in travel time pick.

tion larger than  $-3\%$  in the mid-lower mantle overpredicts SKS traveltime delays after  $137^\circ$  and SKKS traveltime after  $143^\circ$  (for example, models 250km\_vt-3%\_vb-5% and 250km\_vt-3%\_vb-3%, Figures 13a and 13b). We find that only our best fitting model can provide the overall best match to our seismic data.

[28] The observed SKS phases for event DP95/01/03 show a trend of decreasing traveltime delays from 5 s at  $87^\circ$  to 2 s at  $94^\circ$  (Figure 6a). The decrease of SKS traveltime residuals for event DP95/01/03 is consistent with a northeastern flank of the anomaly dipping southwest toward its center. The raw SKS traveltime data are the same as those used by *Ritsema et al.* [1998] and *Ni and Helmberger* [2003b]. The magnitude of the SKS traveltime delays that we attribute to the African Anomaly is, however, different from that in those previous studies which directly attributed the raw data to the anomaly. We do so after making the correction for the effect of event location and origin time, and for the influence of the seismic heterogeneities outside the African Anomaly (see more details in Appendix A1 and A2). For the seismic data from this event, the difference is mainly due to the additional correction for the influence of a high-velocity anomaly in the lowermost mantle beneath South America sampled by

the SKS phases (Appendix A2). This correction was not considered in the previous studies.

[29] In summary, seismic data show that the African Anomaly has a 250-km-thick base extending farther north-east and the northeastern flank of the anomaly tilts toward its apex. The average shear velocity reduction is about  $-5\%$  in the base and about  $-2\%$  in the portion in the mid-lower mantle.

#### 4.2. P Velocity Structure

[30] With the geometry constrained by the S wave data, we investigate P wave velocity structure using traveltime information of direct P, PcP and PcP-P differentials from the same events. The P wave data include P and PcP phases for events SS97/09/05 and SS97/10/05, and direct P for events DP95/01/03, SS95/03/26, SS02/02/10 and SS02/03/09. Our collected P wave data provide good sampling coverage for the African Anomaly (Figure 14). We follow the same procedures we used for the S traveltime analysis, except that we make corrections for the contributions from seismic structure outside the African Anomaly using a global compressional velocity tomographic model [*van der Hilst et al.*, 1997] and the additional correction due to the underestimation of the global compressional tomographic

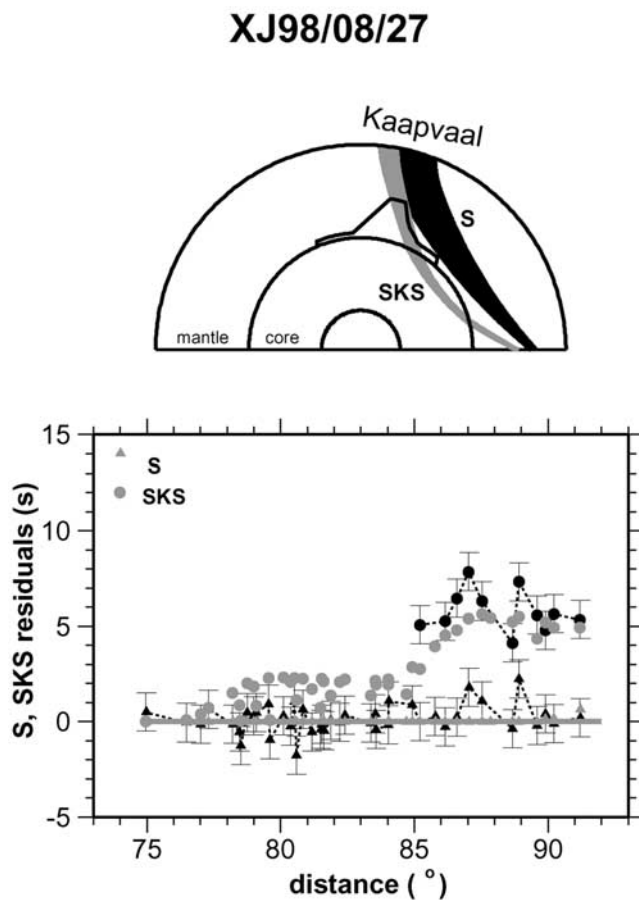


**Figure 11.** (bottom) Observed direct S (black triangles) and SKS (black dots) traveltime residuals with respect to PREM for event XJ98/08/27 and predicted direct S (gray curve) traveltime residuals from the 2-D SH hybrid method waveform modeling results and SKS (gray dots) traveltime residuals from the forward traveltime modeling results based on our best fitting model. (top) Corresponding S and SKS raypaths with respect to the location of the best fitting model, with the paths of no traveltime delays shown in a heavy color. Shown also are the error bars in traveltime pick.

model (see Figure 3c). The direct P waves for events SS97/10/05 and SS97/09/05 show no travel time delay between  $43^\circ$  and  $58^\circ$  (Figure 15a), while the PcP waves show increasing traveltime delays from 0.3 s at  $43^\circ$  to 2 s at  $58^\circ$  (Figure 15b). The PcP-P differential traveltime residuals gradually increase from about 0.15 s at  $43^\circ$  to 1.6–1.8 s at  $58^\circ$  (Figure 15c). The pattern of these P and PcP traveltime delays is the same as seen for the S and ScS traveltime delays for these two events (Figures 4 and 7). The PcP traveltime delays place constraints on the P velocity structure of the southwestern base. The P travel time residuals for event SS95/03/26 show a linear increase to up to 1.4 s at  $73^\circ$  (Figure 15d). Direct P phases are delayed by about 1–2 s for events SS02/02/10 and SS02/03/09 in the whole distance range (Figure 15e). Direct P phases for event DP95/01/03 are delayed by about 1–2.2 s in the whole distance range (Figure 15f). We assume a uniform S to P velocity

perturbation ratio for the African Anomaly and test a series of S to P velocity perturbation ratios from 1:1 to 7:1. We find that a ratio of 3:1 best explains the P traveltime data (see predictions in gray symbols in Figures 15e and 15f). Such a ratio corresponds to a P velocity perturbation of  $-1.67\%$  in the base and  $-1\%$  in the mid-lower mantle portion of the African Anomaly.

## 5. Discussions

[31] In this section, we examine various geometries and shear velocity structure of the African Anomaly and discuss the implications of the inferred geometry and seismic structure of the African Anomaly.

### 5.1. Other Models Examined

[32] We examine two types of representative models: one with its mid-lower mantle portion detached from its base or having a plume-like shape, and the other with both flanks dipping away from the center with a uniform shear velocity reduction for the entire African Anomaly.

#### 5.1.1. A Model With Its Mid-Lower Mantle Portion Detached From Its Base

[33] We test one type of model where the mid-lower mantle portion is detached from the VLVP at the base. Such structures may result from a buoyant, thermal or thermochemical mantle plume, erupting off atop the VLVP at the base of the Earth's mantle. Note that the S waves in our data provide dense coverage through the whole depth range of the African Anomaly (Figure 1a). Our seismic data indicate no structural gap or a shrinking lateral dimension with increasing depth within the African Anomaly. If there were one, our seismic data would have detected it. Here, we present simple examples to illustrate this point. We change our best fitting model by replacing the low-velocity structure in a 200-km radial stripe (between 300 km and 500 km above the CMB) in the middle part of the African Anomaly with PREM-like seismic velocity. Such a structural gap would produce a sharp decrease in traveltime delay at about  $86^\circ$  (Figure 16a), which would have been detected by the S traveltime residuals for event SS02/02/10. A model with a plume-like shape in the mid-lower mantle would predict a decrease of traveltime delays with increasing distance, also inconsistent with the observed traveltime residuals for event SS02/02/10 (Figure 16b). The direct S waves for event SS02/02/10 exhibit continuously increasing traveltime delays with increasing epicentral distance (or turning depth), suggesting that the lateral dimension of the African Anomaly becomes larger with increasing depth.

#### 5.1.2. A Model With Both Flanks Dipping Toward Northeast and a Uniform Shear Velocity Reduction

[34] Recently, Ni *et al.* [2002] proposed a model with both flanks dipping toward northeast and a uniform shear velocity reduction of  $-3\%$ . Their model is derived using mostly seismic phases propagating through the African Anomaly from its western and southwestern directions [Ritsema *et al.*, 1998; Ni *et al.*, 2002; Ni and Helmberger, 2003a, 2003b, 2003c]. Such a model, however, is inconsistent with our data sampling from the northeastern direction. Note that we have very dense sampling coverage in the mid-lower mantle from the northeastern direction (Figure 1a). Note also that the S waves (and the ScS waves at close

## JS97/12/05

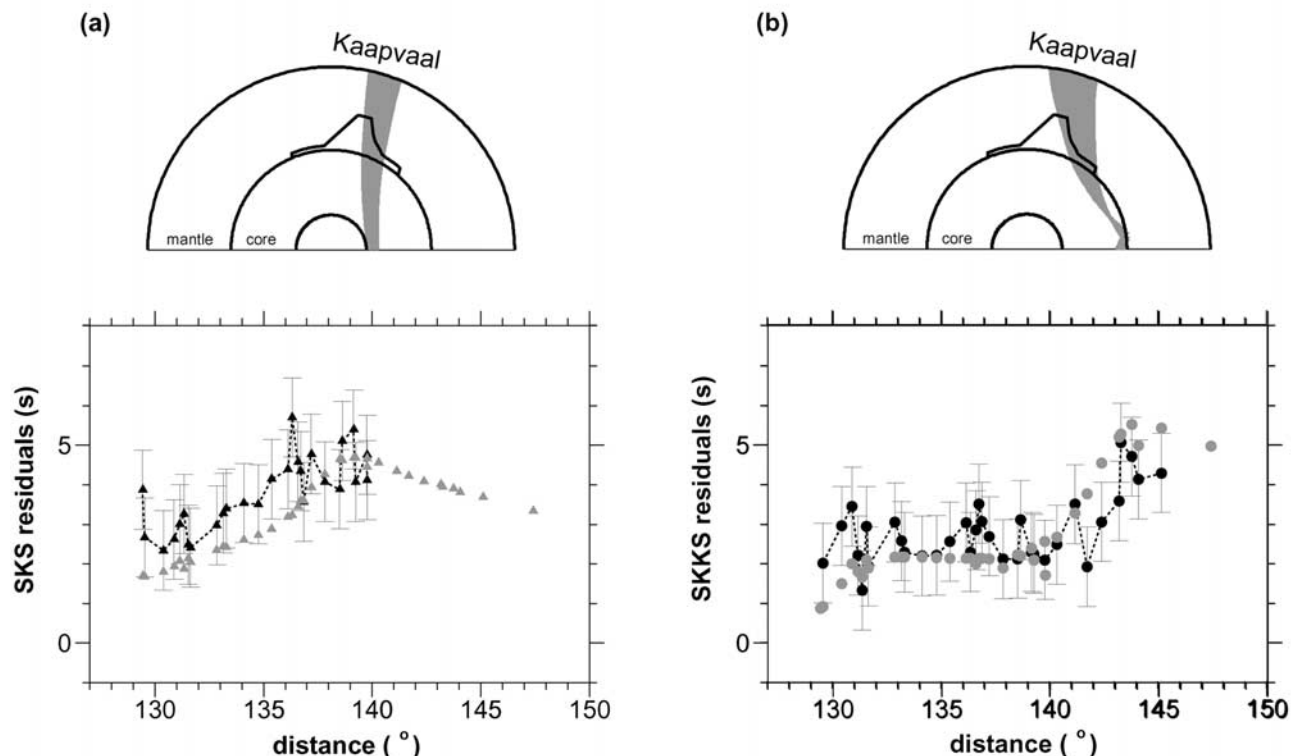


**Figure 12.** (a) (bottom) Observed SKS travel time residuals (black triangles) with respect to PREM for event JS97/12/05 and predicted SKS residuals (gray triangles) from the forward traveltimes modeling results based on our best fitting model. (top) Corresponding SKS raypaths with respect to the location of the best fitting model. (b) Same as Figure 12a, except for SKKS phase of the same event. Shown also in Figures 12a and 12b are the error bars in traveltimes pick.

distances) for events XJ98/08/27, HK97/05/13 and IR98/03/14 show no traveltimes delays (Figures 9, 10, and 11). If the top portion of the anomaly extended farther northeast, it would have been sampled and detected by the direct S waves for these three events and the ScS waves at the close distances for these events. We show an example of such modeling for event XJ98/08/27. With the previously determined geometry for the African Anomaly, the predicted direct S travel time delays would reach about 2, 4 and 6 s at about  $92^\circ$  for assumed shear velocity reductions of  $-1\%$ ,  $-2\%$ , and  $-3\%$ , respectively (Figure 17a). It is evident that even a uniform shear velocity reduction of  $-1\%$  would overpredict S traveltimes residuals. The geometry determined by Ni *et al.* [2002] is also inconsistent with the observed SKS and SKKS traveltimes patterns for event JS97/12/05. For that geometry, the SKS phases would have sampled the middle of the African Anomaly and produced large and relatively uniform traveltimes delays for the whole distance range (dashed line, Figure 17b), while the data show a linear increase of traveltimes delay from  $133^\circ$  to  $137^\circ$  (Figure 17b). The SKKS phases would have sampled the African Anomaly in such a way that they would have produced linearly increasing traveltimes delays from 2 s at  $129^\circ$  to 6 s at  $146^\circ$ , while the data show uniform traveltimes

delays before  $140^\circ$  and a rapid increase of traveltimes delay after  $140^\circ$  (Figure 17c).

### 5.1.3. Similarities and Differences Between Our Preferred Model and Previous Models

[35] Our inferred geometry and shear velocity structure of the African Anomaly has similarities and differences to those inferred from previous studies [Ritsema *et al.*, 1998; Ni *et al.*, 2002; Ni and Helmberger, 2003a, 2003b, 2003c]. The similarities lie in the inferred height, geometry and geographic extent of the basal layer on the southwestern side of the anomaly and average shear velocity reduction in the mid-lower mantle. The major differences lie in the geometry of the northeastern flank, the geographic extent of the basal layer on the northeastern side, and the shear velocity reduction in the bottom portion of the African Anomaly. Compared with previous models, our preferred model indicates that (1) the northeastern flank of the African Anomaly tilts toward the center with the lateral dimension increasing with depth, (2) the basal layer of the African Anomaly extends farther northeast, and (3) the average shear velocity reduction is about  $-5\%$  in the bottom portion of the African Anomaly. These differences result from the fact that more data are used, and corrections for event mislocation and effects of seismic heterogeneities outside

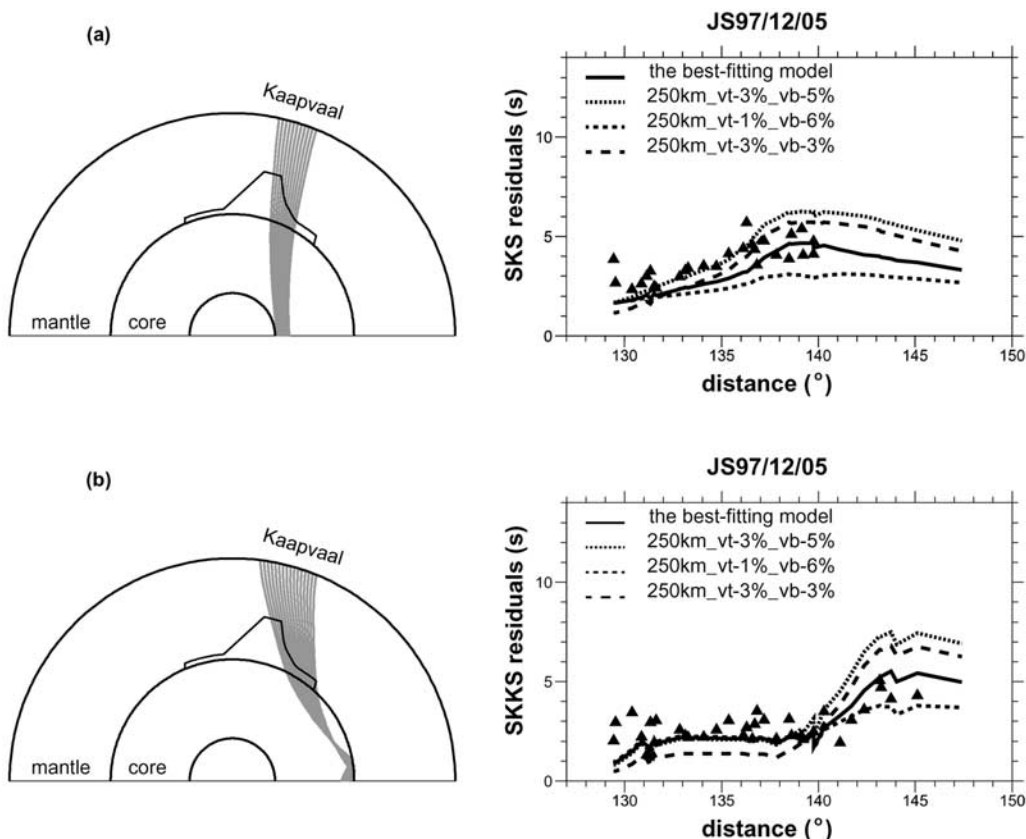


**Figure 13.** (right) Comparisons between observed (a) SKS and (b) SKKS traveltime residuals (black triangles) and predictions from the forward traveltime modeling results based on our best fitting model (solid curves) and three other models (dashed curves) perturbed from the best fitting model with a same thickness of 250 km but different shear velocity reductions in the northeastern basal layer and in the mid-lower mantle portion. The perturbed models include those with shear velocity reductions of  $-3\%$  in the mid-lower mantle and of  $-5\%$  in the base (250km\_vt-3%\_vb-5%), shear velocity reductions of  $-1\%$  in the mid-lower mantle portion and of  $-6\%$  in the base (250km\_vt-1%\_vb-6%), and a uniform shear velocity reduction of  $-3\%$  in both portions (250km\_vt-3%\_vb-3%). (left) Corresponding raypaths with respect to the location and geometry of the testing models.

the anomaly are considered in our study. More discussions on this issue are presented in Appendix A3.

## 5.2. The 3-D Effect of Seismic Wave Propagation

[36] The inferred average shear velocity reduction of  $-5\%$  in the lowermost 150–250 km of the African Anomaly is consistent with the previous result of a linear negative shear velocity gradient from  $-2\%$  (top) to  $-9\%$  to  $-12\%$  (bottom) in the VLVP in the lowermost mantle inferred from 2-D waveform modeling [Wen *et al.*, 2001; Wen, 2001, 2002; Wang and Wen, 2004]. Recent 3-D studies, however, suggested an average shear velocity reduction of  $-3\%$  in the base of the African Anomaly. The differences probably arise from the fact that different frequency contents of the seismic data are used in the seismic modeling. In the 3-D models, the waveforms were band-pass-filtered to a period of 8–15 s [To *et al.*, 2005; Ni *et al.*, 2005]. The large velocity reductions in the 2-D models were inferred from the high-frequency waveform complexities observed in the seismic data (compare broadband data in Figure 6 of Wen [2001] and their filtered components in Figure 2 of To *et al.*

[2005] and Figure 4 of Ni *et al.* [2005] for event 97/09/04). The high-frequency complexities were band-pass-filtered, and synthetics fitting even to the band-passed long-period data were less satisfactory in the 3-D waveform modeling [To *et al.*, 2005; Ni *et al.*, 2005]. The geometry and onset distance of the basal layer have as significant an effect on waveforms as the velocity reductions do [Wen, 2002; Wang and Wen, 2004]. There was no report on the effects of these model parameters on the synthetic waveforms in the 3-D modeling. While one may argue it is difficult to assess the 3-D effects on the broadband seismic data for event 97/09/04, the large negative shear velocity gradient was also inferred from the detailed 2-D waveform modeling of the broadband seismic data sampling various directions of the anomaly. Most of the seismic data that were used in our 2-D modeling were not used in constraining the 3-D models. For example, our previous models were constrained by the seismic data from events 97/09/02 and 97/11/28, and many other seismic data sampling the African Anomaly from the western side [Wen *et al.*, 2001; Wen, 2001, 2002; Wang and Wen, 2004]. On the basis of the inferred geographic distri-

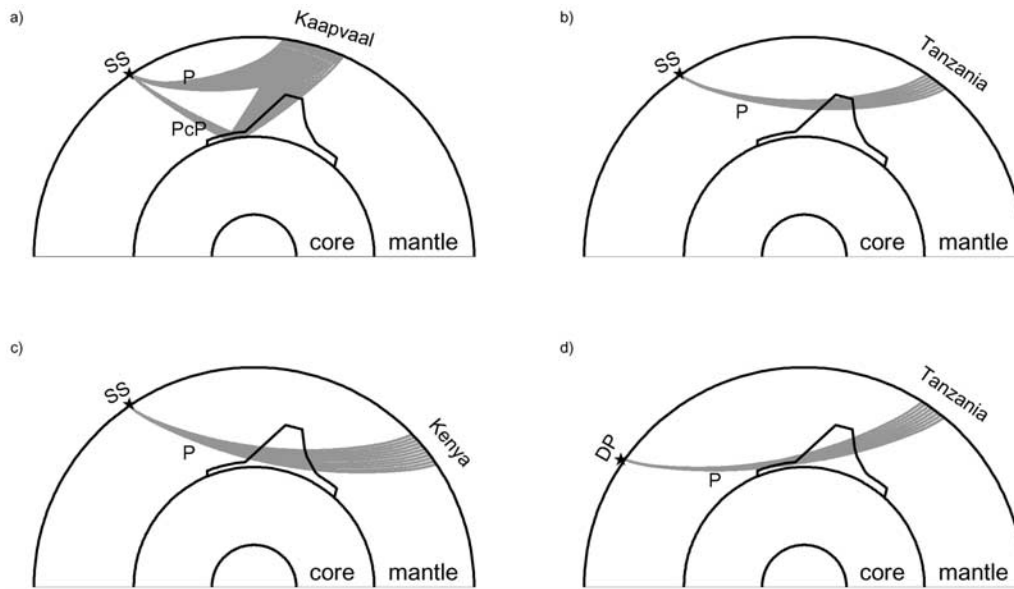


**Figure 14.** Raypaths of P and PcP waves sampling the African Anomaly with respect to the location of the best fitting model: (a) direct P and PcP for events SS97/10/05 and SS97/09/05, (b–d) direct P waves for event SS95/03/26 (Figure 14b), events SS02/02/10 and SS02/03/09 (Figure 14c), and event DP95/01/03 (Figure 14d).

bution of the VLVP [Wang and Wen, 2004], for some sampling paths such as the propagation paths for event 97/09/02 [Wen *et al.*, 2001; Wen, 2002; Wang and Wen, 2004], the 3-D effects on wave propagation should be small.

[37] The 3-D seismic structure of the African Anomaly in the mid-lower mantle is not clear due to the data coverage provided by the current distribution of seismic stations and earthquakes. So it is, at present, difficult to study the effect of the 3-D structure in the mid-lower mantle on the seismic wave propagation.

### 5.3. Implications for the “Bell-Like” Geometry and Seismic Structure

[38] The geometry of the African Anomaly indicates that the portions of the anomaly in the mid-lower mantle and near the CMB are integral components, and the whole African Anomaly is compositionally distinct. Geodynamic modeling results show that the bell-like geometric shape in which both sides tilt toward the center of the African Anomaly further indicates that the compositional buoyancy of the African Anomaly is large and the African Anomaly is geologically stable. The geometry of the African Anomaly is similar to the thermal-chemical convection models presented by Ni *et al.* [2002], with a buoyancy number  $B = 0.23$  and a Rayleigh number  $Ra = 10^7$  [Ni *et al.*, 2002, Figure 3B or Figure 3E]. For these models, a denser basal layer at the bottom of the mantle is entrained upward. Because the density buoyancy associated with the compositional change is larger than that of thermal effect, the compositional anomaly becomes geologically stable and the entrainment creates a bell-like geometry. Imposing a tectonic plate velocity would make the slope of the northeastern side of the anomaly a little steeper than that of the other side [Ni *et al.*, 2002, Figure 3E]. The geometry of the African Anomaly is consistent with above models. Our

modeling results also indicate that the geometries such as those in Figures 3A and 3F of Ni *et al.* [2002], which have a detached mid-lower mantle portion or have two flanks tilting toward the same direction, are inconsistent with our seismic observations (sections 4.1.1 and 4.1.2). These models can be produced when the compositional buoyancy is small ( $B < 0.22$ ) and the compositional anomaly is geologically unstable.

## 6. Conclusions

[39] We constrain the geometry and the S and P velocity structure of the African Anomaly along a great arc from the East Pacific Rise to the Japan Sea, based on waveform and traveltime forward modeling of direct S, direct P, Sdiff, ScS, PcP, SKS and SKKS phases recorded by three temporary broadband PASSCAL seismic arrays employed in Africa between 1994 and 2002, the Tanzania seismic array (1994–1995), the Kaapvaal seismic array (1997–1999), and the Ethiopia/Kenya seismic array (2000–2002), for earthquakes occurring in the East Pacific Rise, Drake Passage, South Sandwich islands, Iran, Hindu Kush, Xinjiang and the Japan Sea. In order to accurately account for the contributions from the African Anomaly, we make corrections for the effects of earthquake mislocation and the seismic heterogeneities outside the African Anomaly. Seismic data indicate that the African Anomaly extends 1300 km above the CMB with its apex located at around ( $25^\circ$  S,  $27^\circ$  E) beneath southern Africa, exhibits a bell-like shape in the mid-lower mantle with both flanks dipping toward its center, and has a 150- to 250-km-thick and 4000-km-wide basal layer extending farther in both the northeastern and the southwestern directions. Seismic data can best be explained by average shear velocity reductions of  $-5\%$  in the base and  $-2\%$  to  $-3\%$  in the mid-lower mantle portion and a uniform S to P

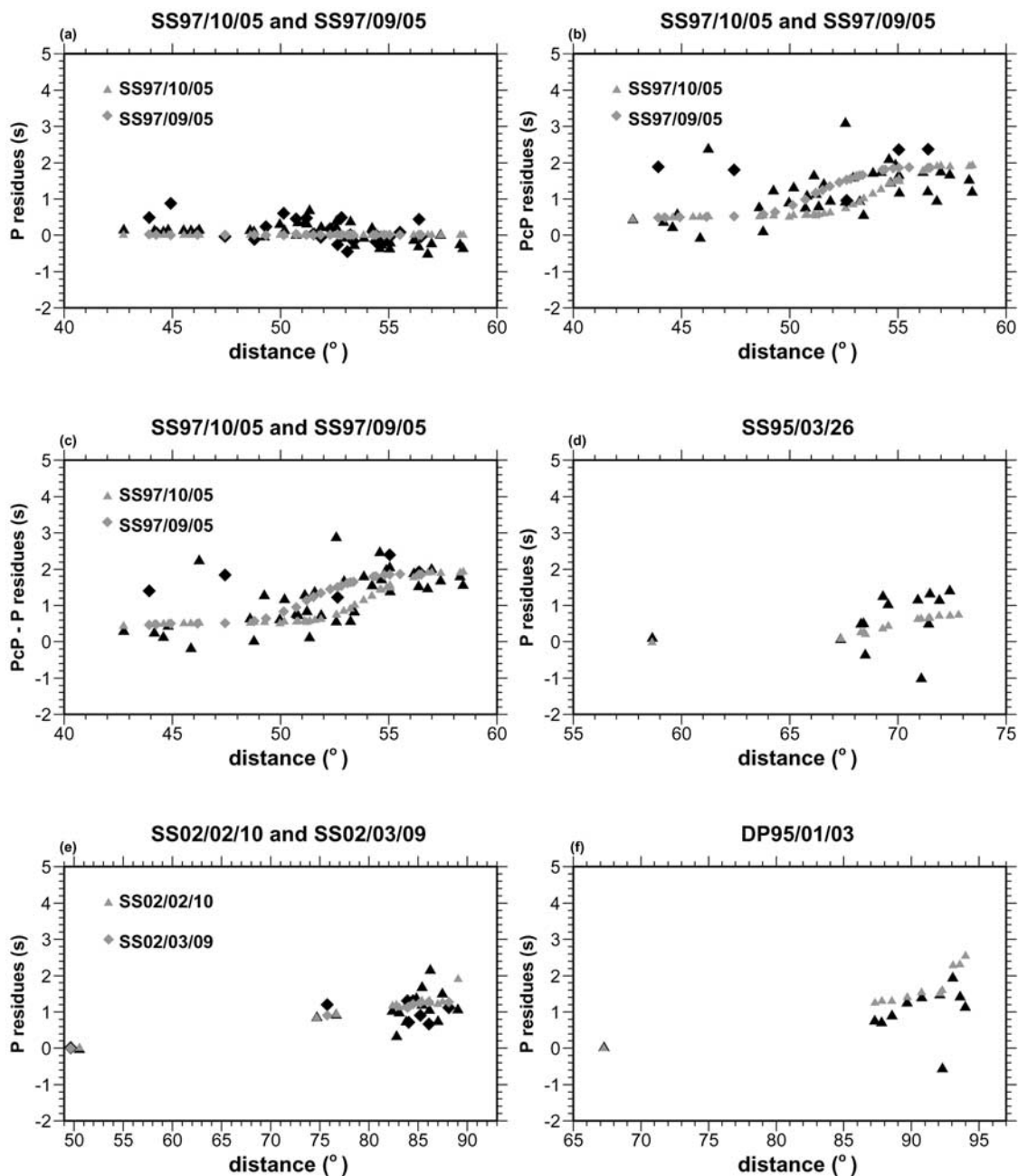


**Figure 15.** Comparisons between observed direct P or PcP traveltime residuals with respect to PREM and predictions from the forward traveltime modeling results based on the best fitting model for six events (see Figure 14 for their corresponding raypaths). (a) Observed direct P traveltime residuals for events SS97/10/05 (black triangles) and SS97/09/05 (black diamonds) with respect to PREM and predictions (gray triangles and diamonds). (b) Observed PcP residuals for events SS97/10/05 (black triangles) and SS97/09/05 (black diamonds) with respect to PREM and predictions (gray triangles and diamonds). (c) Observed PcP-P differential traveltime residuals for events SS97/10/05 (black triangles) and SS97/09/05 (black diamonds) with respect to PREM and predictions (gray triangles and diamonds). (d) Observed direct P traveltime residuals (black triangles) for event SS95/03/26 with respect to PREM and predictions (gray triangles). The observation at about  $59^\circ$  is for GSN station LSZ. (e) Observed direct P traveltime residuals for events SS02/02/10 (black triangles) and SS02/03/09 (black diamonds) with respect to PREM and predictions (gray triangles and diamonds). The two observations at  $50^\circ$  are for GSN stations BOSA and TSUM. (f) Observed direct P traveltime residuals (black triangles) for event DP95/01/03 with respect to PREM and predictions (gray triangles). The observation at  $67^\circ$  is for GSN station BOSA.

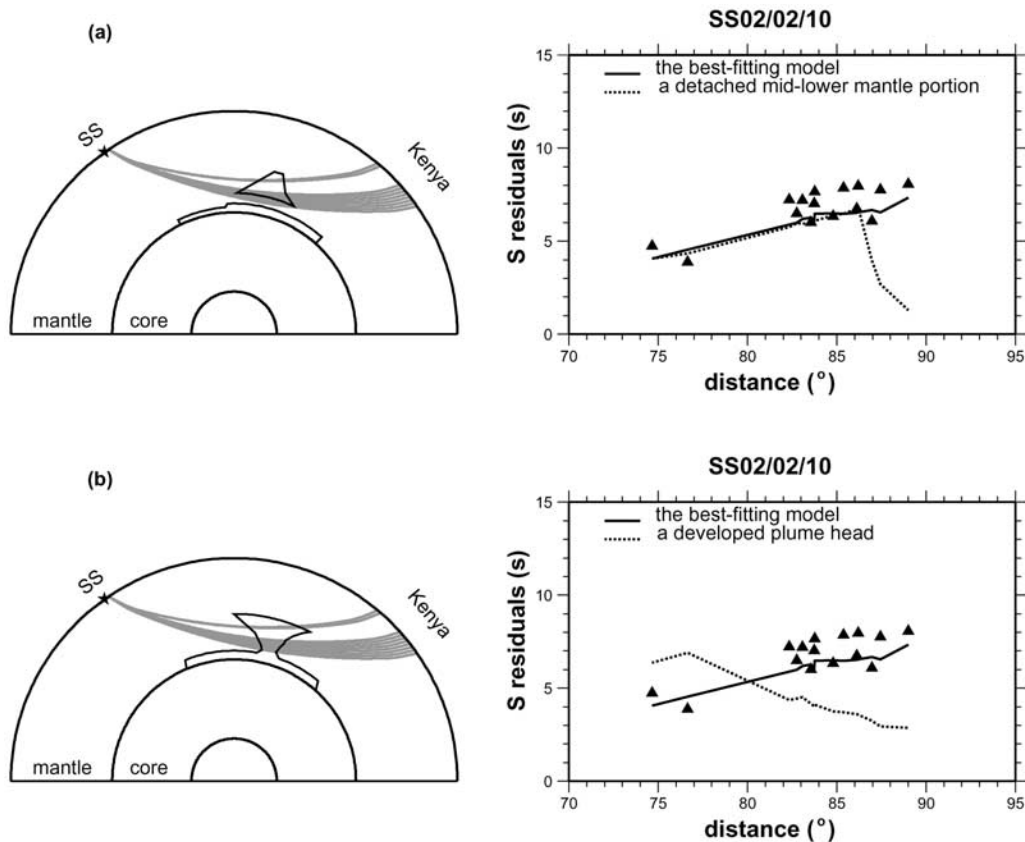


**Figure 16.** (right) Comparisons between observed direct S traveltime residuals (black triangles) for event SS02/02/10 and predictions from the forward traveltime modeling results based on our best fitting model (solid curve) and (a) one detached model (dashed curve) with its portion in the mid-lower mantle separated from the base by 200 km and (b) a plume-like model in the mid-lower mantle. (left) Corresponding S ray paths with respect to the location of the detached model (Figure 16a) and the plume-like model (Figure 16b).

velocity perturbation ratio of 3:1. Seismic data also indicate that the mid-lower mantle portion of the African Anomaly and its broad base at the CMB are integral components. The lateral dimension of the anomaly increases with increasing depth and there is no structural gap within the anomaly. The structural and velocity features suggest that the African Anomaly is compositionally distinct and geologically stable.

## Appendix A: Preliminary Data Processing

### A1. Earthquake Relocation

[40] Because our S wave data have better global coverage, we use travel times of direct S phases recorded by the GSN between  $20^\circ$  and  $90^\circ$  to relocate all the earthquakes used in this study (Figures A1–A4). The relocation process is that, within a  $10^\circ$  by  $10^\circ$  by 10 s space-time range (longitude, latitude, and time) centered at the original event longitude, latitude, and origin time presented in the Harvard CMT catalog, we carry out a grid search with an interval of  $0.1^\circ$  in longitude and  $0.1^\circ$  in latitude and 0.1 s in origin time for the best fitting location and origin time. The best fitting location and origin time is the one that predicts the smallest root mean square of the differences between the observed direct S traveltime and the calculated direct S traveltime

based on the assumed new location and origin time and a global shear velocity tomographic model [Grand *et al.*, 1997]. When permitted, as in the case for event HK97/05/13, we relocate event depth by using the differential traveltimes between S and the surface reflection (sS) phases. Relocation results are presented in Table 1. The relocation significantly reduces the traveltime misfits for the GSN observations (Figures A1–A4).

### A2. Additional Corrections for the SKS Traveltime Residuals Observed for Event DP95/01/03

[41] Additional corrections are made to the SKS traveltimes observed for event DP95/01/03. Note that the SKS waves for event DP95/01/03 propagate through a fast velocity zone in the source-side lowermost mantle beneath South America (Figure 1a). Our employed global tomographic model overall underestimates the influence of this fast velocity anomaly by about 2 s. This value is obtained from the comparison of the observed traveltimes of the S phases recorded by the Kaapvaal array for a seismic event (event 97/12/13, data not shown) and the predictions based on the seismic tomographic model. Event 97/12/13 occurs geographically between event DPR97/06/10 and event DP95/01/03. The S waves for that event propagates from outside the fast velocity anomaly at close distances to inside

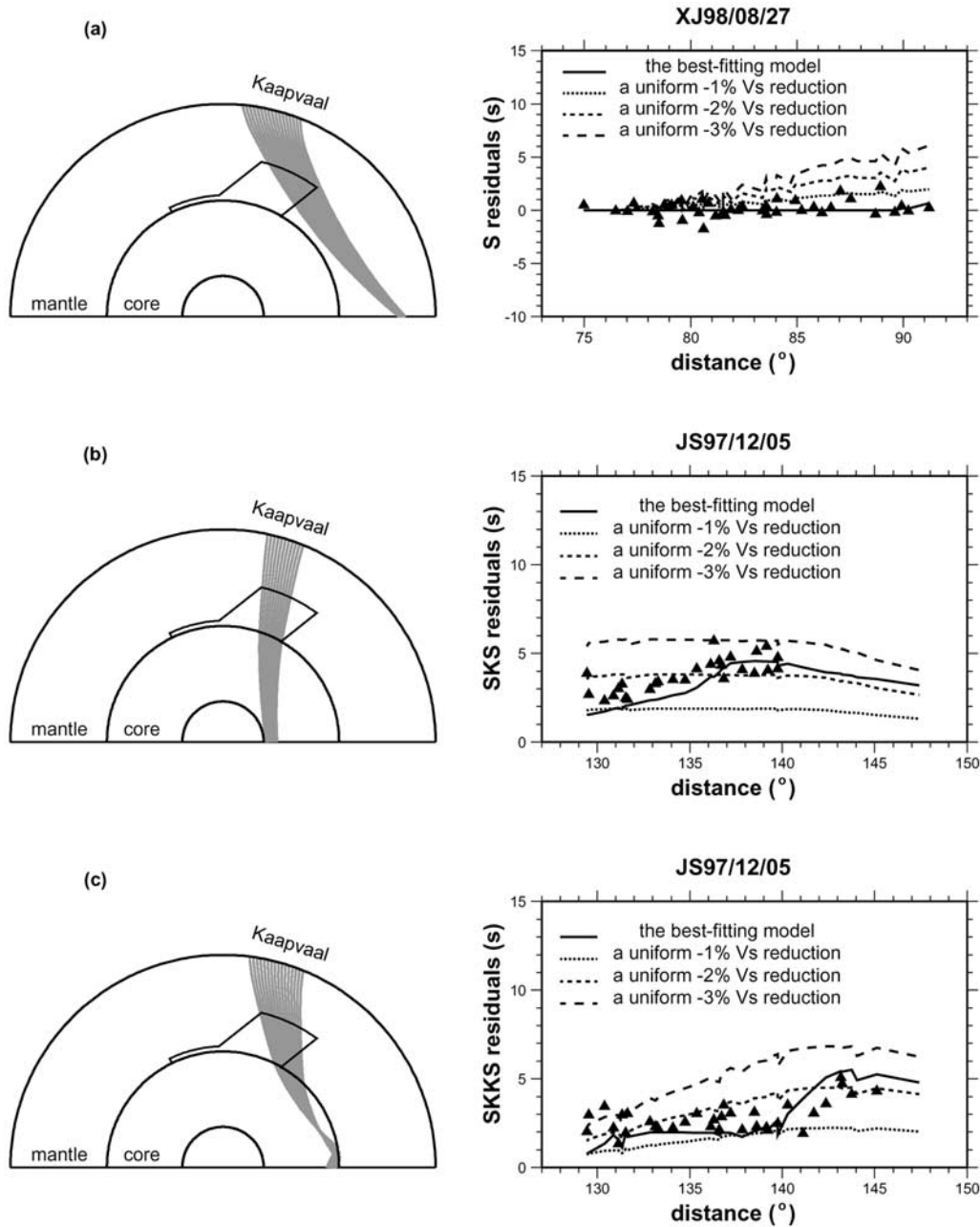


**Figure 17.** (right) Comparisons between observed traveltime residuals (black triangles) and predictions from the forward traveltime modeling results based on our best fitting model (solid curves) and models (dashed curves) with a previously determined geometry [Ni *et al.*, 2002] and various uniform shear velocity reductions, for these phases and events: (a) direct S and event XJ98/08/27; (b) SKS phase and event JS97/12/05; and (c) SKKS phase and event JS97/12/05. (left) Corresponding raypaths with respect to the location and geometry of the testing models.

it at large distances. The S waves propagating inside the fast velocity anomaly arrive about 2 s earlier than those traveling outside. The travel times of the SKS phases for event DP95/01/03 are thus corrected by an additional 2 s.

### A3. Detailed Discussions on the Similarities and Differences Between Our Preferred Model and Previous Models

[42] The similarities in the inferred height, geometry and geographic extent of the basal layer on the southwestern

side of the anomaly and shear velocity reduction in the mid-lower mantle between our model and previous models are probably due to the fact that similar seismic data were employed in deriving these models [Ritsema *et al.*, 1998; Ni and Helmberger, 2003b, 2003c, and this study]. Ni and Helmberger [2003b] constrained the southwestern flank of the anomaly using the traveltime residuals for the SKS phases observed in the Kaapvaal array for two events (EPR97/05/29 and EPR97/09/03) occurring in the East Pacific Rise, while we do it by using the traveltime residuals

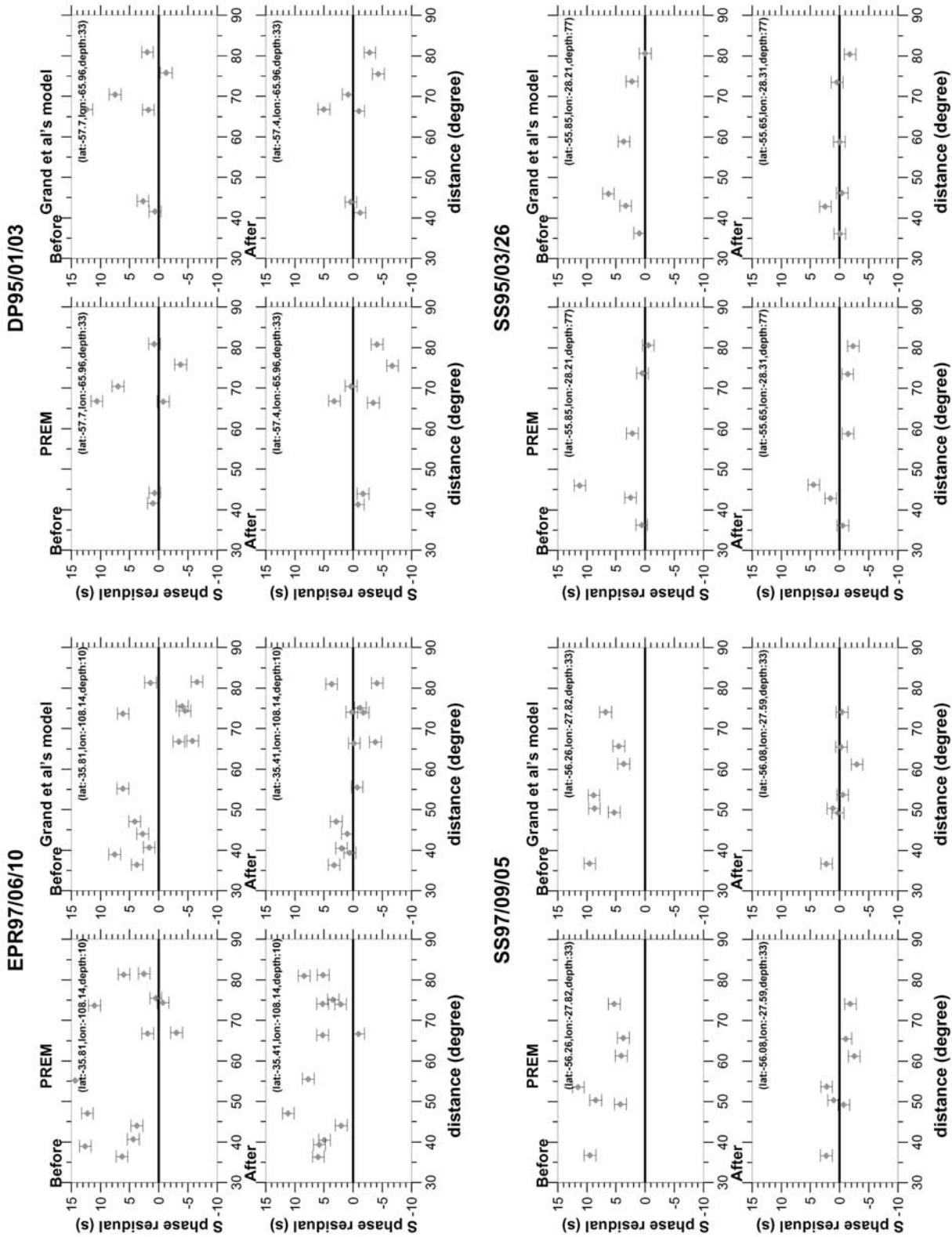


**Figure A1.** (left) S traveltime residuals (diamonds) with respect to PREM before and after earthquake relocation, and (right) S traveltime residuals (diamonds) with respect to *Grand et al.*'s [1997] model before and after earthquake relocation, for events EPR97/06/10, DP95/01/03, SS97/09/05, and SS95/03/26.

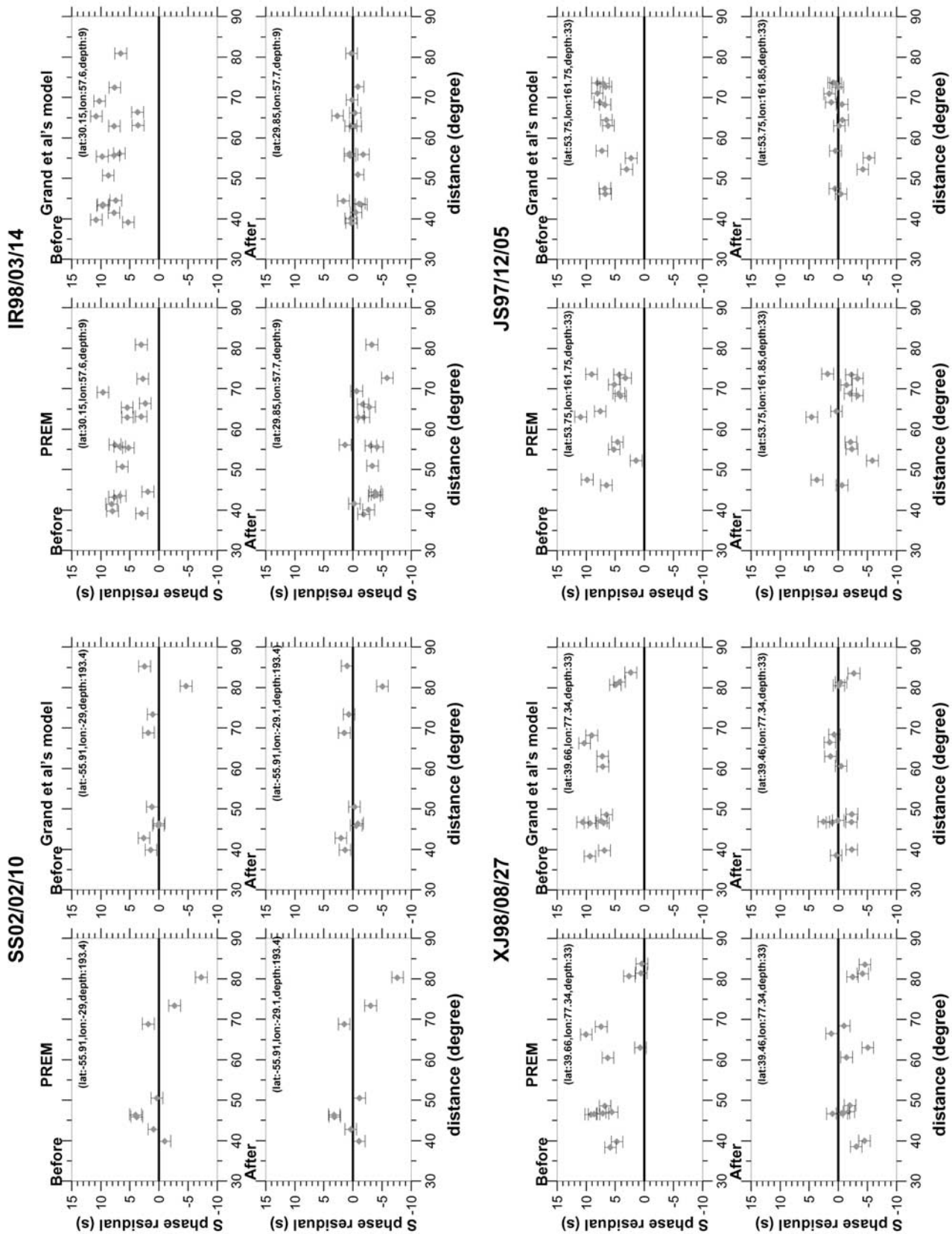


Figure A2. Same as Figure A1 except for events SS02/02/10, IR98/03/14, XJ98/08/27, and JS97/12/05.

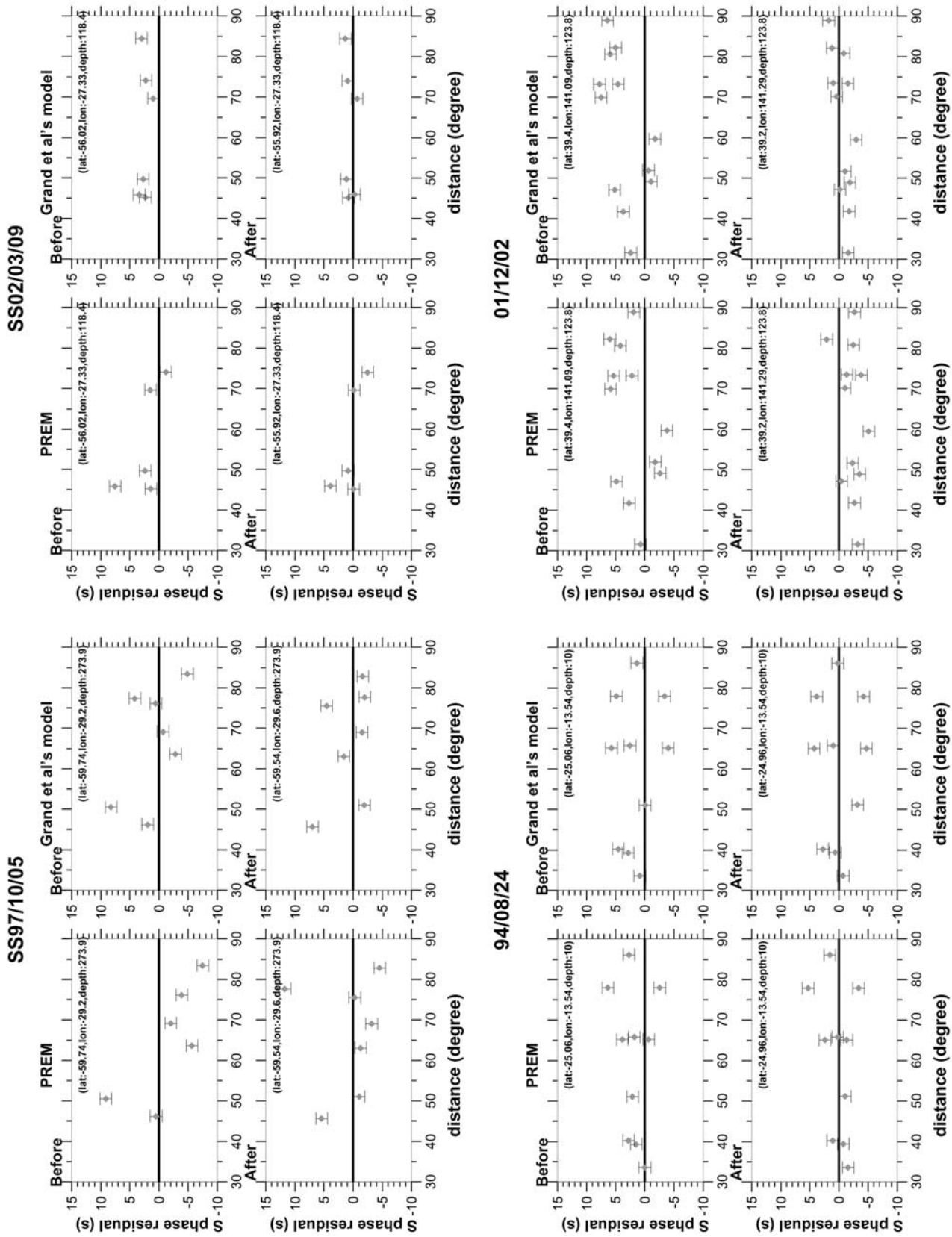
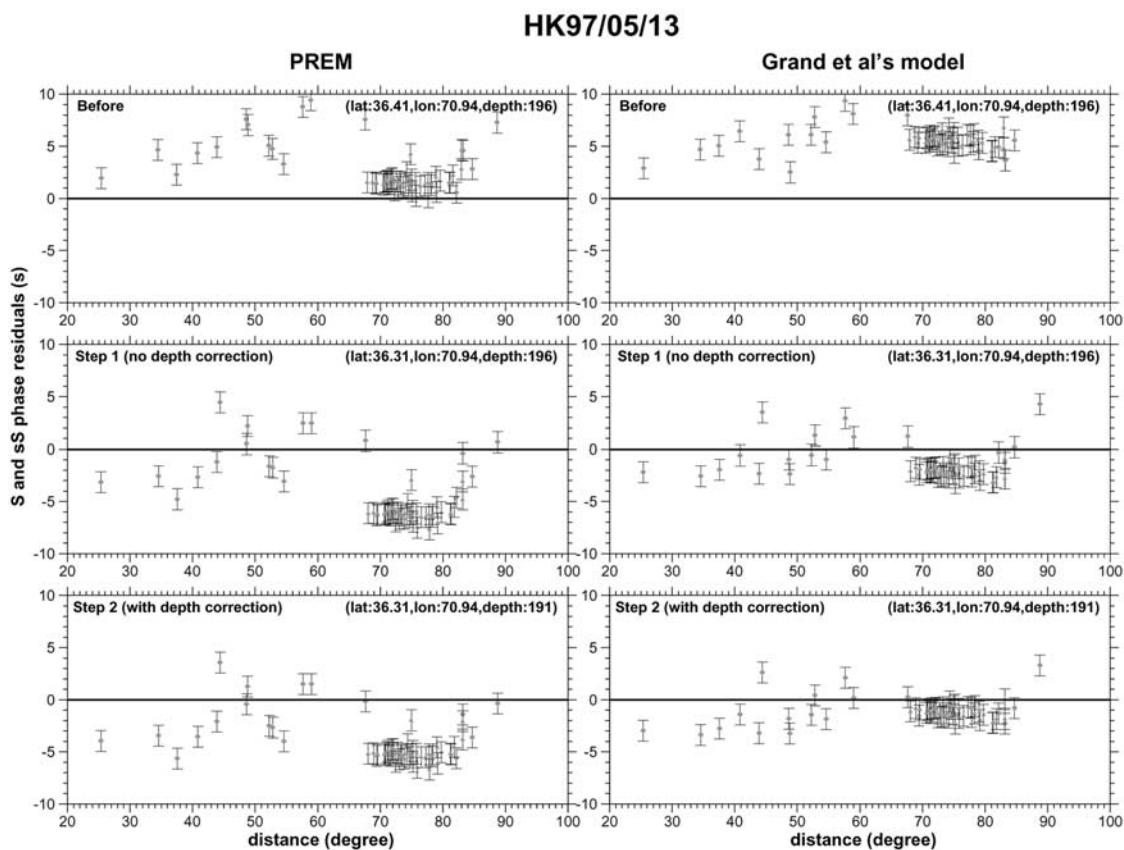


Figure A3. Same as Figure A1 except for events SS97/10/05, SS02/03/09, 94/08/24, and 01/12/02.



**Figure A4.** Direct S (diamonds) and sS (triangles) traveltime residuals with respect to (left) PREM and (right) *Grand et al.*'s [1997] model: (top) raw data, (middle) after correction for event latitude and longitude (step 1), and (bottom) after further correction for focal depth (step 2).

for the SKS phases recorded by the Kaapvaal array for event EPR97/06/10 occurring in a similar region. Event EPR97/05/29 is slightly north of event EPR97/06/10, while event EPR97/09/03 is slightly south of event EPR97/06/10. *Ni and Helmberger* [2003a] reported that the SKS traveltime delays increase from about 0 s before  $99^\circ$  to 5 s at  $102^\circ$  for event EPR97/05/29, and from about 0 s at  $102^\circ$  to 5 s at  $108^\circ$  for event EPR97/09/03. The SKS traveltime residuals for event EPR97/06/10 reported in our study show a rapid increase from about 1–2 s before  $101^\circ$  to 6.7 s at  $107^\circ$  (Figure 5). Our observed SKS traveltime pattern for event EPR97/06/10 is similar to those observed for events EPR97/09/03 and EPR97/05/29. Our inferred geometry on the southwestern side of the anomaly is overall consistent with that inferred by *Ni and Helmberger* [2003b]. The height of the anomaly was constrained by using the traveltime residuals of the S waves recorded by the Tanzania array for an event occurring in South Sandwich islands (event 94/07/25) in the previous study [*Ritsema et al.*, 1998]. It is constrained by using the traveltime delays after  $69^\circ$  for event SS95/03/26 in our study (Figure 4). Both events have similar characteristics, so the inferred height of the African Anomaly is similar between the studies. The basal layer on the southwestern side of the anomaly was constrained using the Sdiff phases for event EPR97/06/10 in the study by *Ni and Helmberger* [2003c]. The geographic location and geometry of the basal layer on the southwestern side of the anomaly are constrained by the ScS-S differential traveltimes for

events SS97/09/05 and SS95/03/26, SKS traveltimes for event DP95/01/03 and the Sdiff waveforms for event EPR97/06/10 (Figures 4, 5, 6, and 7) in our study. There is some difference in the traveltime residuals reported between the two studies, as our data are corrected for event mislocation and the effects of seismic heterogeneity outside the African Anomaly. As a result, our inferred slope of the southwestern flank is less steep than that in the previous studies. Overall, however, the inferred height, geometry in the southwestern flank and shear velocity reduction in the top portion of the anomaly are similar between the studies.

[43] The differences in the inferred geometry of the northeastern flank of the anomaly, geographic extent of the basal layer on the northeastern side, and shear velocity reduction in the bottom portion of the African Anomaly result from the fact that more data are used in this study, especially those sampling the northeastern direction. The models by *Ni et al.* [2002] suggest that the northeastern flank of the African Anomaly tilts outward from its center, the basal layer ends coincident with its mid-lower mantle extension in the northeast and the shear velocity reduction at the bottom of the anomaly is  $-3\%$ . Our model indicates that the northeastern flank of the African Anomaly dips toward its center, a 250-km-thick basal layer extends farther northeast and the average shear velocity reduction in the lowermost mantle is about  $-5\%$ . In deriving the geometry of the northeastern flank of the anomaly, the previous studies used the ScS-S differential travel times from an event occurring

in the Hindu Kush [Ritsema *et al.*, 1998] and the SKS traveltimes and waveforms recorded by the Tanzania seismic array for one event occurring in the Drake Passage [Ritsema *et al.*, 1998] and one event in South America [Ni *et al.*, 2002]. Among their data, the SKS phases sample the anomaly from the southwestern direction; only the S and ScS phases for the event occurring in the Hindu Kush sample the anomaly from the northeastern direction, but they were not discussed in detail in the previous studies. Besides, the ScS-S time residuals place weak constraints on the geometry of the northeastern flank of the anomaly in the mid-lower mantle, as ScS and S waves have similar propagation paths in the mid-lower mantle. The geometry of the northeastern flank of the anomaly in our model is constrained using the traveltimes residuals for the S and ScS waves recorded by the Kaapvaal seismic array for three events occurring in Iran, Hindu Kush and Xinjiang and the travel time residuals for the SKS, SKKS phases sampling from the northeastern direction recorded by the Kaapvaal array for an event occurring in the Japan Sea (Figure 1a). All these observations were not used in the previous studies. These additional observations place tight constraints on the geometry, geographic extent and velocity structure on the northeastern side of the anomaly (see discussions in section 4.1.3). The difference in the inferred average velocity reductions in the lowermost mantle is due to our data effectively placing bounds on the thickness of the basal layer to be about 150–200 km on the southwestern side by the Sdiff waveforms observed for event EPR97/06/10 (Figure 5a) and the S traveltimes for event DP95/01/03 (Figure 6a), and that additional ScS, SKS and SKKS phases for events IR98/03/14, XJ980827 and JS97/12/05 sampling the northeastern side are used in our study (Figures 10b, 11, and 12).

[44] Our model is also consistent with the seismic data that were used in the previous studies to infer the geometry of the northeastern flank of the anomaly [Ritsema *et al.*, 1998; Ni and Helmberger, 2003b, 2003c]. The ScS-S differential travel time residuals reported by Ritsema *et al.* [1998] are around zero for an event occurring in Hindu Kush, consistent with our model. In fact, our model is constrained by using much denser ScS-S differential traveltimes. Our ScS-S differential travel times show no residuals at close distances, similar to the GSN observations presented in the study by Ritsema *et al.* [1998]. Our data also reveal increasing positive residuals at large distances for events IR98/03/14 and HK97/05/13 which are consistent with the existence of a basal layer extending farther northeast. The primary constraints on the geometry of the northeastern side of the anomaly in the previous studies are the SKS traveltimes and waveform complexities from events occurring in Drake Passage and South America. The SKS traveltimes for the Drake Passage event are also used in our study and our model explains the observation well (Figure 6). As mentioned in the main text, additional correction is needed to account for the effects of the seismic heterogeneities outside the African Anomaly and of a high-velocity anomaly beneath South America. Those effects were not considered in the previous studies, but are taken into account in our study (Appendix A2).

[45] Previous studies reported a change of SKS waveform complexity from simple wavelets to complex ones and

traveltimes variation from normal to a delay of 5 s over an epicentral distance range of about  $3^\circ$  for an event occurring in South America (event 94/10/20) recorded by the Tanzania seismic array [Ni *et al.*, 2002]. These changes were interpreted as due to the SKS waves propagating along a sharp eastern side of the anomaly that extends obliquely 1500 km upward from the core-mantle boundary. The sampled azimuth of their SKS phases is about  $15^\circ$  away from the great arc studied in this study. It is not clear to us what corrections were made in their reported SKS traveltimes residuals, as the SKS exit points at the core-mantle boundary are clearly within the VLVP. The SKS phases for other earthquakes occurring in the North Atlantic Ocean, South America and the Japan Sea (see the SKS traveltimes residuals for events H, F and Q in Figure 1b of Wang and Wen [2004]), whose exit points at the CMB are north, east and west of those of the SKS phases for event 94/10/20 reported by Ni *et al.* [2002], all clearly show nearly uniform traveltimes delays, consistent with the existence of a basal layer extending farther east. Our observed SKS traveltimes for the same event and those after the event relocation and traveltimes corrections, do not show such an abrupt SKS traveltimes variation. The observed SKS waveform complexities were interpreted as the effect of multipathing of the SKS phases propagating 1500 km along the eastern side of the anomaly. It is interesting to note that the SKS waveform complexities for event 94/10/20 are observed at stations MITU, KIBA, KIBE, MTOR, SING and possibly KONDA, MBWE. These stations are located near the geographic boundary of the Tanzania craton. Similar SKS waveform complexities are also observed for these same stations for other events occurring in different parts of the South American subduction zone. We suggest it is more likely that the waveform complexities observed at these stations are caused by heterogeneous seismic structure in the shallow mantle. The SKS data have poor vertical resolution in resolving the seismic structure, as the SKS phases propagate nearly vertically. Even if the SKS waveform complexities are caused by heterogeneity in the deep mantle, they may also be explained by localized seismic anomalies near the CMB [Wen and Helmberger, 1998]. Meanwhile, SKKS-SKS differential traveltimes of the same event show a smooth variation with recording distances that cannot be predicted by a sharp transition of shear velocity reduction at the boundary of two sides of the mid-lower mantle portion of the African Anomaly as reported by Ni *et al.* [2002]. In short, our model is consistent with the SKS data for event 94/10/20.\*

[46] **Acknowledgments.** We are grateful to the IRIS for supplying data. The seismic data used in this paper were collected as part of the Kaapvaal, Tanzania, and Ethiopia/Kenya research projects. We also thank the principal academic collaborators and investigators in all three projects for their efforts in collecting the seismic data and Andy Nyblade for generously making the Ethiopia/Kenya data available to us before they were released. We thank Michael Ritzwoller, the Associate Editor, and two anonymous reviewers for comments and suggestions. This work is supported by NSF grants EAR0001232 and EAR0309859.

## References

- Dziewonski, A., and D. L. Anderson (1981), Preliminary reference Earth model, *Phys. Earth Planet. Inter.*, 25, 297–356.  
 Fouch, M. J., P. Silver, and D. E. James (1999), Probing for shear wave anisotropy in the lowermost mantle beneath the Atlantic and Indian oceans, *Eos Trans. AGU*, 80(46), Fall Meet. Suppl., F759.

\*The sentence is correct here. The article as originally published is online.

- Grand, S. P., R. D. van der Hilst, and S. Widiyantoro (1997), Global seismic tomography: A snapshot of convection in the Earth, *GSA Today*, 7, 1–7.
- Gurnis, M., J. X. Mitrovica, J. Ritsema, and H. van Heijst (2000), Constraining mantle density structure using geological evidence of surface uplift rates: The case of the African Superplume, *Geochem. Geophys. Geosyst.*, 1(7), doi:10.1029/1999GC000035.
- Ishii, M., and J. Tromp (1999), Normal-mode and free-air gravity constraints on lateral variations in velocity and density of the Earth’s mantle, *Science*, 285, 1231–1236.
- Li, X. D., and B. Romanowicz (1996), Global mantle shear velocity model developed using nonlinear asymptotic coupling theory, *J. Geophys. Res.*, 101, 22,245–22,273.
- Lithgow-Bertelloni, C., and P. G. Silver (1998), Dynamic topography, plate driving forces and the African superswell, *Nature*, 395, 269–272.
- Masters, G., S. Johnson, G. Laske, and H. Bolton (1996), A shear velocity model of the mantle, *Philos. Trans. R. Soc. London*, 354, 1385–1411.
- Masters, G., G. Laske, H. Bolton, and A. Dziewonski (2000), Earth’s deep interior: Mineral physics and tomography from the atomic to the global scale, in *Earth’s Deep Interior: Mineral Physics and Tomography From the Atomic to the Global Scale*, *Geophys. Monogr. Ser.*, vol. 117, edited by S. Karato et al., pp. 63–87, AGU, Washington, D. C.
- Ni, S., and D. V. Helmberger (2003a), Ridge-like lower mantle structure beneath South Africa, *J. Geophys. Res.*, 108(B2), 2094, doi:10.1029/2001JB001545.
- Ni, S., and D. V. Helmberger (2003b), Seismological constraints on the South African superplume; could be the oldest distinct structure on Earth, *Earth Planet. Sci. Lett.*, 206, 119–131.
- Ni, S., and D. V. Helmberger (2003c), Further constraints on the African superplume structure, *Phys. Earth Planet. Inter.*, 140, 243–251.
- Ni, S., X. Ding, D. V. Helmberger, and M. Gurnis (1999), Low-velocity structure beneath Africa from forward modeling, *Earth Planet. Sci. Lett.*, 170, 497–507.
- Ni, S., E. Tan, M. Gurnis, and D. V. Helmberger (2002), Sharp sides to the African super plume, *Science*, 296, 1850–1852.
- Ni, S., D. V. Helmberger, and J. Tromp (2005), Three-dimensional structure of the African superplume from waveform modelling, *Geophys. J. Int.*, 161, 283–294.
- Ritsema, J., S. Ni, and D. V. Helmberger (1998), Evidence for strong shear velocity reductions and velocity gradients in the lower mantle beneath Africa, *Geophys. Res. Lett.*, 25, 4245–4248.
- Ritsema, J., H. J. van Heijst, and J. H. Woodhouse (1999), Complex shear wave velocity structure imaged beneath Africa and Iceland, *Science*, 286, 1925–1928.
- Simmons, N. A., and S. P. Grand (2002), Partial melting in the deepest mantle, *Geophys. Res. Lett.*, 29(11), 1552, doi:10.1029/2001GL013716.
- Su, W. J., R. L. Woodward, and A. M. Dziewonski (1992), Degree 12 model of shear velocity heterogeneity in the mantle, *J. Geophys. Res.*, 99, 6945–6980.
- To, A., B. Romanowicz, Y. Capdeville, and N. Takeuchi (2005), 3D effects of sharp boundaries at the borders of the African and Pacific Superplumes: Observation and modeling, *Earth Planet. Sci. Lett.*, 233, 137–153.
- van der Hilst, R. D., S. Widiyantoro, and E. R. Engdahl (1997), Evidence for deep mantle circulation from global tomography, *Nature*, 386, 578–584.
- Wang, Y., and L. Wen (2004), Mapping the geometry and geographic distribution of a very low velocity province at the base of the Earth’s mantle, *J. Geophys. Res.*, 109, B10305, doi:10.1029/2003JB002674.
- Wen, L. (2001), Seismic evidence for a rapidly varying compositional anomaly at the base of the Earth’s mantle beneath the Indian Ocean, *Earth Planet. Sci. Lett.*, 194, 83–95.
- Wen, L. (2002), An SH hybrid method and shear velocity structures in the lowermost mantle beneath the central Pacific and South Atlantic Oceans, *J. Geophys. Res.*, 107(B3), 2055, doi:10.1029/2001JB000499.
- Wen, L., and D. V. Helmberger (1998), A 2D P-SV hybrid method and its application to localized structures near the core-mantle boundary, *J. Geophys. Res.*, 103, 17,901–17,918.
- Wen, L., P. Silver, D. James, and R. Kuehnel (2001), Seismic evidence for a thermo-chemical boundary layer at the base of the Earth’s mantle, *Earth Planet. Sci. Lett.*, 189, 141–153.

---

L. Wen, Department of Geosciences, State University of New York at Stony Brook, Stony Brook, NY 11794, USA. (lwen@notes.cc.sunysb.edu)  
 Y. Wang, CGGVeritas, 10300 Town Park Drive, Houston, TX 77072, USA. (yi.wang@cggeveritas.com)